Control Optimization

Dehaeze Thomas

April 5, 2025

Contents

When controlling a MIMO system (specifically parallel manipulator such as the Stewart platform?)

Several considerations:

- Section 1: How to most effectively use/combine multiple sensors
- Section 2: How to decouple a system
- Section 3: How to design the controller

1 Multiple Sensor Control

Look at what was done in the introduction Stewart platforms: Control architecture

Different control objectives:

- Vibration Control

- Position Control

Sometimes, the two objectives are simultaneous, as is the case for the NASS, in that case it is usually beneficial to combine multiple sensors in the control architecture.

Explain why multiple sensors are sometimes beneficial:

- collocated sensor that guarantee stability, but is still useful to damp modes outside the bandwidth of the controller using sensor measuring the performance objective

- Noise optimization

Several architectures (Figure 1.1):

- HAC-LAC (Figure 1.1a) [1], [2], [3], [4], [5], [6]

- Sensor Fusion (Figure 1.1c) [7], [8], [9]

- Two Sensor control (Figure 1.1b) [7], [9], [10], [11]

- ☐ Explain basic idea for three strategies:

  - HAC-LAC: sequential control.

  - Sensor Fusion: use different sensors in different frequency regions for different reasons: noise, robustness, ...

  - Two sensor control: idea is to have the maximum control on how both sensors are utilized. Theoretically, this could give the best performances (as sensor fusion is a special case of two sensor control). But it may be more complex to tune and analyze.

Comparison between "two sensor control" and "sensor fusion" is given in [10].

The use of multiple sensors have already been used for the Stewart platform. Table 1.1

Cascaded control / HAC-LAC Architecture was already discussed during the conceptual phase. This is a very comprehensive approach that proved to give good performances.
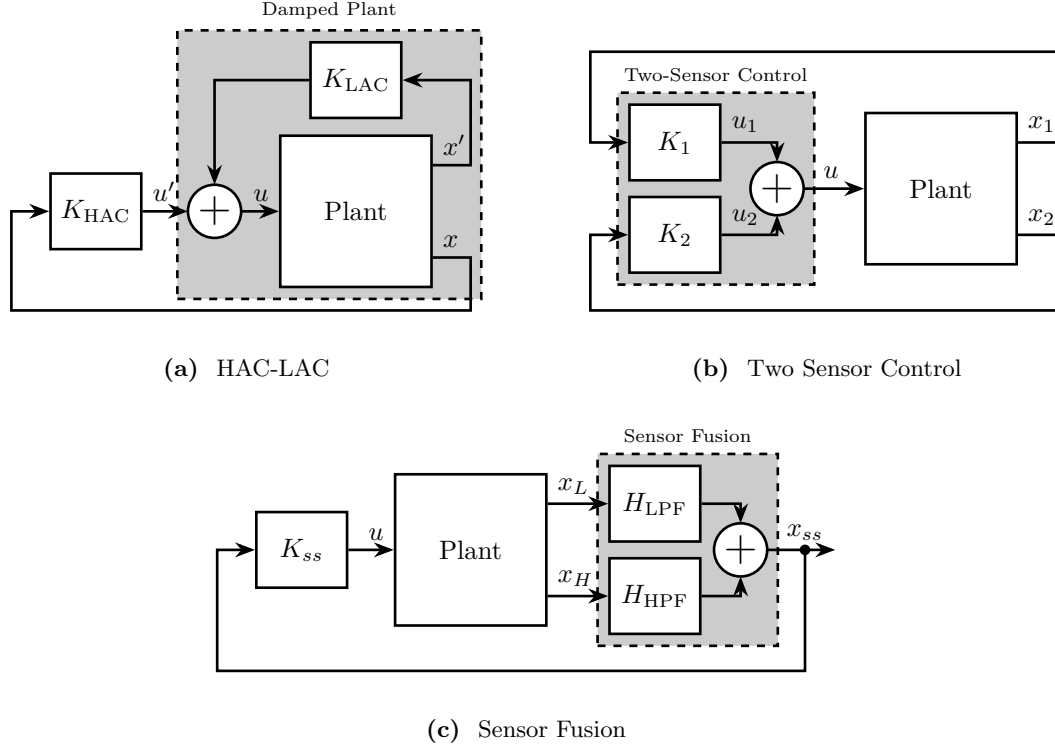
(a) HAC-LAC

(b) Two Sensor Control

(c) Sensor Fusion

Figure 1.1: Different control strategies when using multiple sensors. High Authority Control / Low Authority Control (a). Sensor Fusion (c). Two-Sensor Control (b)

Table 1.1: Review of Stewart platforms integrating multiple sensors

Actuators	Sensors	Control
Magnetostrictive	Force (collocated), Accelerometers	Two layers: Decentralized IFF, Robust Adaptive Control
Piezoelectric	Force Sensor + Accelerometer	HAC-LAC (IFF + FxLMS)
Voice Coil	Accelerometer (collocated), ext. Rx/Ry sensors	Cartesian acceleration feedback (isolation) + 2DoF pointing control (external sensor)
Voice Coil	Geophone + Eddy Current (Struts, collocated)	Decentralized (Sky Hook) + Centralized (modal) Control
Voice Coil	Force sensors (struts) + accelerometer (cartesian)	Decentralized Force Feedback + Centralized H2 control based on accelerometers
Voice Coil	Force (HF) and Inertial (LF)	**Sensor Fusion**, **Two Sensor Control**
Voice Coil	Force (HF) and Inertial (LF)	**Sensor Fusion**, LQG, Decentralized
Piezoelectric	Force, Position	Vibration isolation, Model-Based, Modal control: 6x PI controllers
Voice Coil	Force, LVDT, Geophones	LQG, Force + geophones for vibration, LVDT for pointing
Voice Coil	Force	IFF, centralized (decouple) + decentralized (coupled)

On the other hand of the spectrum, the two sensor approach yields to more control design freedom. But it is also more complex.

In this section, we wish to study if sensor fusion can be an option for multi-sensor control:

- may be used to optimize the noise characteristics

- optimize the dynamical uncertainty

1.1 Sensor fusion - Introduction

Measuring a physical quantity using sensors is always subject to several limitations. First, the accuracy of the measurement is affected by several noise sources, such as electrical noise of the conditioning electronics being used. Second, the frequency range in which the measurement is relevant is bounded by the bandwidth of the sensor. One way to overcome these limitations is to combine several sensors using a technique called "sensor fusion" [18]. Fortunately, a wide variety of sensors exists, each with different characteristics. By carefully choosing the fused sensors, a so called "super sensor" is obtained that can combines benefits of the individual sensors.

In some situations, sensor fusion is used to increase the bandwidth of the measurement [19], [20], [21]. For instance, in [19] the bandwidth of a position sensor is increased by fusing it with an accelerometer providing the high frequency motion information. For other applications, sensor fusion is used to obtain an estimate of the measured quantity with lower noise [22], [23], [24], [25]. More recently, the fusion of sensors measuring different physical quantities has been proposed to obtain interesting properties for control [11], [26]. In [26], an inertial sensor used for active vibration isolation is fused with a sensor collocated with the actuator for improving the stability margins of the feedback controller.

Practical applications of sensor fusion are numerous. It is widely used for the attitude estimation of several autonomous vehicles such as unmanned aerial vehicle [27], [28], [29] and underwater vehicles [30], [31]. Naturally, it is of great benefits for high performance positioning control as shown in [11], [19], [20], [21]. Sensor fusion was also shown to be a key technology to improve the performance of active vibration isolation systems [8]. Emblematic examples are the isolation stages of gravitational wave detectors [26], [32] such as the ones used at the LIGO [22], [23] and at the Virgo [33].

There are mainly two ways to perform sensor fusion: either using a set of complementary filters [34] or using Kalman filtering [35]. For sensor fusion applications, both methods are sharing many relationships [25], [35], [36], [37]. However, for Kalman filtering, assumptions must be made about the probabilistic character of the sensor noises [25] whereas it is not the case with complementary filters. Furthermore, the advantages of complementary filters over Kalman filtering for sensor fusion are their general applicability, their low computational cost [36], and the fact that they are intuitive as their effects can be easily interpreted in the frequency domain.

A set of filters is said to be complementary if the sum of their transfer functions is equal to one at all frequencies. In the early days of complementary filtering, analog circuits were employed to physically realize the filters [34]. Analog complementary filters are still used today [11], [38], but most of the time they are now implemented digitally as it allows for much more flexibility.

Several design methods have been developed over the years to optimize complementary filters. The easiest way to design complementary filters is to use analytical formulas. Depending on the application,

the formulas used are of first order [11], [28], [39], second order [27], [29], [40] or even higher orders [19], [20], [26], [40], [41].

As the characteristics of the super sensor depends on the proper design of the complementary filters [42], several optimization techniques have been developed. Some are based on the finding of optimal parameters of analytical formulas [21], [29], [37], while other are using convex optimization tools [22], [23] such as linear matrix inequalities [30]. As shown in [24], the design of complementary filters can also be linked to the standard mixed-sensitivity control problem. Therefore, all the powerful tools developed for the classical control theory can also be used for the design of complementary filters. For instance, in [29] the two gains of a Proportional Integral (PI) controller are optimized to minimize the noise of the super sensor.

The common objective of all these complementary filters design methods is to obtain a super sensor that has desired characteristics, usually in terms of noise and dynamics. Moreover, as reported in [20], [24], phase shifts and magnitude bumps of the super sensors dynamics can be observed if either the complementary filters are poorly designed or if the sensors are not well calibrated. Hence, the robustness of the fusion is also of concern when designing the complementary filters. Although many design methods of complementary filters have been proposed in the literature, no simple method that allows to specify the desired super sensor characteristic while ensuring good fusion robustness has been proposed.

Fortunately, both the robustness of the fusion and the super sensor characteristics can be linked to the magnitude of the complementary filters [42]. Based on that, this work introduces a new way to design complementary filters using the $\mathcal{H}_\infty$ synthesis which allows to shape the complementary filters' magnitude in an easy and intuitive way.

1.2 Sensor Fusion and Complementary Filters Requirements

Complementary filtering provides a framework for fusing signals from different sensors. As the effectiveness of the fusion depends on the proper design of the complementary filters, they are expected to fulfill certain requirements. These requirements are discussed in this section.

Sensor Fusion Architecture   A general sensor fusion architecture using complementary filters is shown in Figure 1.2 where several sensors (here two) are measuring the same physical quantity x. The two sensors output signals $\hat{x}_1$ and $\hat{x}_2$ are estimates of x. These estimates are then filtered out by complementary filters and combined to form a new estimate $\hat{x}$.

The resulting sensor, termed as "super sensor", can have larger bandwidth and better noise characteristics in comparison to the individual sensors. This means that the super sensor provides an estimate $\hat{x}$ of x which can be more accurate over a larger frequency band than the outputs of the individual sensors.

The complementary property of filters $H_1(s)$ and $H_2(s)$ implies that the sum of their transfer functions is equal to one (1.1). That is, unity magnitude and zero phase at all frequencies.
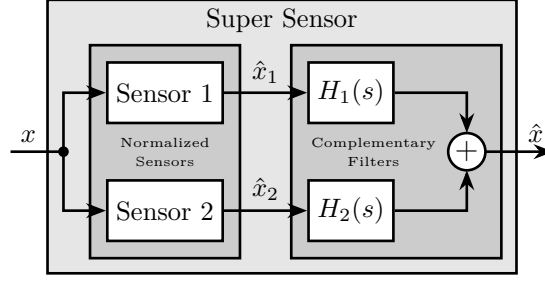
$$H_1(s) + H_2(s) = 1 \tag{1.1}$$

7

Figure 1.2: Schematic of a sensor fusion architecture using complementary filters.

Sensor Models and Sensor Normalization In order to study such sensor fusion architecture, a model for the sensors is required. Such model is shown in Figure 1.3a and consists of a linear time invariant (LTI) system $G_i(s)$ representing the sensor dynamics and an input n_i representing the sensor noise. The model input x is the measured physical quantity and its output $\tilde{x}_i$ is the "raw" output of the sensor.

Before filtering the sensor outputs $\tilde{x}_i$ by the complementary filters, the sensors are usually normalized to simplify the fusion. This normalization consists of using an estimate $\hat{G}_i(s)$ of the sensor dynamics $G_i(s)$, and filtering the sensor output by the inverse of this estimate $\hat{G}_i^{-1}(s)$ as shown in Figure 1.3b. It is here supposed that the sensor inverse $\hat{G}_i^{-1}(s)$ is proper and stable. This way, the units of the estimates $\hat{x}_i$ are equal to the units of the physical quantity x. The sensor dynamics estimate $\hat{G}_i(s)$ can be a simple gain or a more complex transfer function.
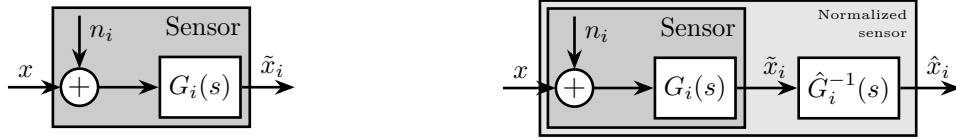
(a) Basic sensor model consisting of a noise input n_i and a linear time invariant transfer function $G_i(s)$

(b) Normalized sensors using the inverse of an estimate $\hat{G}$

Figure 1.3: Sensor models with and without normalization.

Two normalized sensors are then combined to form a super sensor as shown in Figure 1.4. The two sensors are measuring the same physical quantity x with dynamics $G_1(s)$ and $G_2(s)$, and with *uncorrelated* noises n_1 and n_2. The signals from both normalized sensors are fed into two complementary filters $H_1(s)$ and $H_2(s)$ and then combined to yield an estimate $\hat{x}$ of x. The super sensor output $\hat{x}$ is therefore described by (1.2).

$$\hat{x} = \left(H_1(s)\hat{G}_1^{-1}(s)G_1(s) + H_2(s)\hat{G}_2^{-1}(s)G_2(s)\right)x + H_1(s)\hat{G}_1^{-1}(s)G_1(s)n_1 + H_2(s)\hat{G}_2^{-1}(s)G_2(s)n_2 \quad (1.2)$$

Noise Sensor Filtering First, suppose that all the sensors are perfectly normalized (1.3). The effect of a non-perfect normalization will be discussed afterwards.

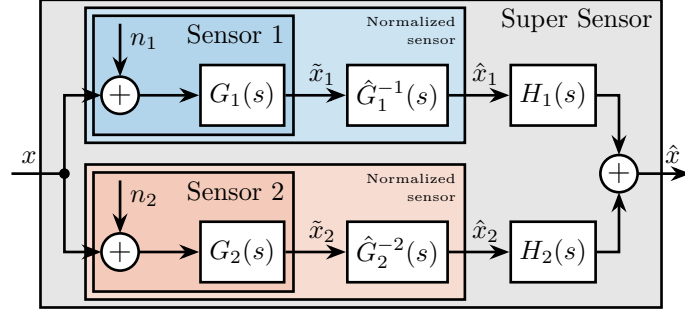$$\frac{\hat{x}_i}{x} = \hat{G}_i(s)G_i(s) = 1 \tag{1.3}$$

Figure 1.4: Sensor fusion architecture with two normalized sensors.

Provided (1.3) is verified, the super sensor output $\hat{x}$ is then equal to x plus the filtered noise of both sensors (1.4). From (1.4), the complementary filters $H_1(s)$ and $H_2(s)$ are shown to only operate on the noise of the sensors. Thus, this sensor fusion architecture permits to filter the noise of both sensors without introducing any distortion in the physical quantity to be measured. This is why the two filters must be complementary.

$$\hat{x} = x + H_1(s)n_1 + H_2(s)n_2 \tag{1.4}$$

The estimation error δx, defined as the difference between the sensor output $\hat{x}$ and the measured quantity x, is computed for the super sensor (1.5).

$$\delta x \triangleq \hat{x} - x = H_1(s)n_1 + H_2(s)n_2 \tag{1.5}$$

As shown in (1.6), the Power Spectral Density (PSD) of the estimation error $\Phi_{\delta x}$ depends both on the norm of the two complementary filters and on the PSD of the noise sources Φ_{n_1} and Φ_{n_2}.

$$\Phi_{\delta x}(\omega) = |H_1(j\omega)|^2 \, \Phi_{n_1}(\omega) + |H_2(j\omega)|^2 \, \Phi_{n_2}(\omega) \tag{1.6}$$

If the two sensors have identical noise characteristics, $\Phi_{n_1}(\omega) = \Phi_{n_2}(\omega)$, a simple averaging ($H_1(s) = H_2(s) = 0.5$) is what would minimize the super sensor noise. This is the simplest form of sensor fusion with complementary filters.

However, the two sensors have usually high noise levels over distinct frequency regions. In such case, to lower the noise of the super sensor, the norm $|H_1(j\omega)|$ has to be small when $\Phi_{n_1}(\omega)$ is larger than $\Phi_{n_2}(\omega)$ and the norm $|H_2(j\omega)|$ has to be small when $\Phi_{n_2}(\omega)$ is larger than $\Phi_{n_1}(\omega)$. Hence, by properly shaping the norm of the complementary filters, it is possible to minimize the noise of the super sensor.

Sensor Fusion Robustness In practical systems the sensor normalization is not perfect and condition (1.3) is not verified.

In order to study such imperfection, a multiplicative input uncertainty is added to the sensor dynamics (Figure 1.5a). The nominal model is the estimated model used for the normalization $\hat{G}_i(s)$, $\Delta_i(s)$ is any stable transfer function satisfying $|\Delta_i(j\omega)| \leq 1$, $\forall\omega$, and $w_i(s)$ is a weighting transfer function representing the magnitude of the uncertainty. The weight $w_i(s)$ is chosen such that the real sensor

dynamics $G_i(j\omega)$ is contained in the uncertain region represented by a circle in the complex plane, centered on 1 and with a radius equal to $|w_i(j\omega)|$.

As the nominal sensor dynamics is taken as the normalized filter, the normalized sensor can be further simplified as shown in Figure 1.5b.
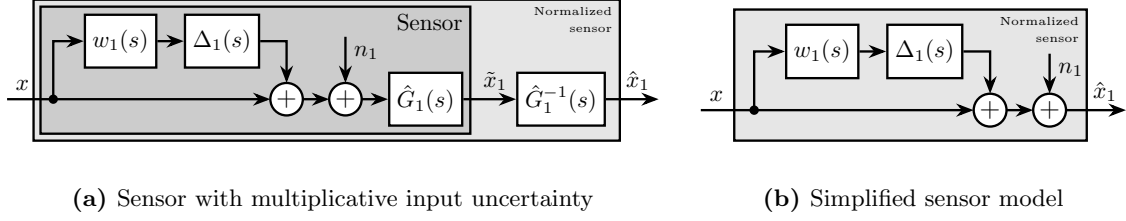

(a) Sensor with multiplicative input uncertainty

(b) Simplified sensor model

Figure 1.5: Sensor models with dynamical uncertainty

The sensor fusion architecture with the sensor models including dynamical uncertainty is shown in Figure 1.6a. The super sensor dynamics (1.7) is no longer equal to 1 and now depends on the sensor dynamical uncertainty weights $w_i(s)$ as well as on the complementary filters $H_i(s)$. The dynamical uncertainty of the super sensor can be graphically represented in the complex plane by a circle centered on 1 with a radius equal to $|w_1(j\omega)H_1(j\omega)| + |w_2(j\omega)H_2(j\omega)|$ (Figure 1.6b).

$$\frac{\hat{x}}{x} = 1 + w_1(s)H_1(s)\Delta_1(s) + w_2(s)H_2(s)\Delta_2(s) \tag{1.7}$$

(a) Sensor Fusion Architecture
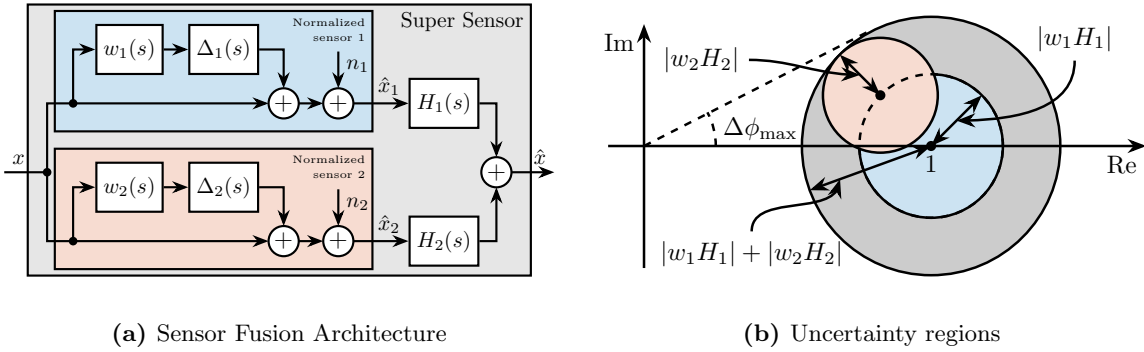
(b) Uncertainty regions

Figure 1.6: Sensor fusion architecture with sensor dynamics uncertainty (a). Uncertainty region (b) of the super sensor dynamics in the complex plane (grey circle). The contribution of both sensors 1 and 2 to the total uncertainty are represented respectively by a blue circle and a red circle. The frequency dependency ω is here omitted.

The super sensor dynamical uncertainty, and hence the robustness of the fusion, clearly depends on the complementary filters' norm. For instance, the phase $\Delta\phi(\omega)$ added by the super sensor dynamics at frequency ω is bounded by $\Delta\phi_{\max}(\omega)$ which can be found by drawing a tangent from the origin to the uncertainty circle of the super sensor (Figure 1.6b) and that is mathematically described by (1.8).

$$\Delta\phi_{\max}(\omega) = \arcsin\left(|w_1(j\omega)H_1(j\omega)| + |w_2(j\omega)H_2(j\omega)|\right) \tag{1.8}$$

As it is generally desired to limit the maximum phase added by the super sensor, $H_1(s)$ and $H_2(s)$ should be designed such that $\Delta\phi$ is bounded to acceptable values. Typically, the norm of the complementary

filter $|H_i(j\omega)|$ should be made small when $|w_i(j\omega)|$ is large, i.e., at frequencies where the sensor dynamics is uncertain.

1.3 Complementary Filters Shaping

As shown in Section 1.2, the noise and robustness of the super sensor are a function of the complementary filters' norm. Therefore, a synthesis method of complementary filters that allows to shape their norm would be of great use. In this section, such synthesis is proposed by writing the synthesis objective as a standard $\mathcal{H}_\infty$ optimization problem. As weighting functions are used to represent the wanted complementary filters' shape during the synthesis, their proper design is discussed. Finally, the synthesis method is validated on an simple example.

Synthesis Objective   The synthesis objective is to shape the norm of two filters $H_1(s)$ and $H_2(s)$ while ensuring their complementary property (1.1). This is equivalent as to finding proper and stable transfer functions $H_1(s)$ and $H_2(s)$ such that conditions (1.9a), (1.9b) and (1.9c) are satisfied. $W_1(s)$ and $W_2(s)$ are two weighting transfer functions that are carefully chosen to specify the maximum wanted norm of the complementary filters during the synthesis.

$$H_1(s) + H_2(s) = 1 \tag{1.9a}$$

$$|H_1(j\omega)| \leq \frac{1}{|W_1(j\omega)|} \quad \forall\omega \tag{1.9b}$$

$$|H_2(j\omega)| \leq \frac{1}{|W_2(j\omega)|} \quad \forall\omega \tag{1.9c}$$

Shaping of Complementary Filters using $\mathcal{H}_\infty$ synthesis   The synthesis objective can be easily expressed as a standard $\mathcal{H}_\infty$ optimization problem and therefore solved using convenient tools readily available. Consider the generalized plant $P(s)$ shown in Figure 1.7a and mathematically described by (1.10).

$$\begin{bmatrix} z_1 \\ z_2 \\ v \end{bmatrix} = P(s) \begin{bmatrix} w \\ u \end{bmatrix}; \quad P(s) = \begin{bmatrix} W_1(s) & -W_1(s) \\ 0 & W_2(s) \\ 1 & 0 \end{bmatrix} \tag{1.10}$$

Applying the standard $\mathcal{H}_\infty$ synthesis to the generalized plant $P(s)$ is then equivalent as finding a stable filter $H_2(s)$ which based on v, generates a signal u such that the $\mathcal{H}_\infty$ norm of the system in Figure 1.7b from w to $[z_1, \ z_2]$ is less than one (1.11).

$$\left\| \begin{matrix} (1 - H_2(s)) \, W_1(s) \\ H_2(s)W_2(s) \end{matrix} \right\|_\infty \leq 1 \tag{1.11}$$

By then defining $H_1(s)$ to be the complementary of $H_2(s)$ (1.12), the $\mathcal{H}_\infty$ synthesis objective becomes equivalent to (1.13) which ensures that (1.9b) and (1.9c) are satisfied.
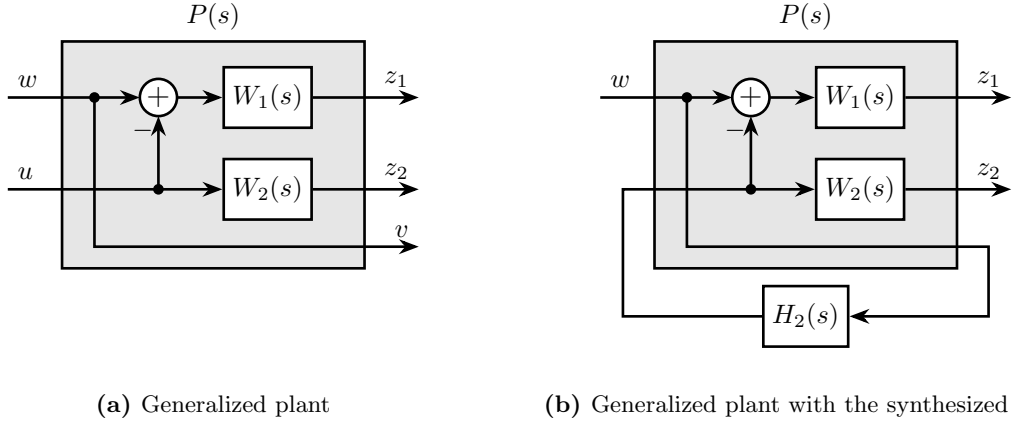
(a) Generalized plant   **(b)** Generalized plant with the synthesized filter

Figure 1.7: Architecture for the $\mathcal{H}_\infty$ synthesis of complementary filters

$$H_1(s) \triangleq 1 - H_2(s) \tag{1.12}$$

$$\left\| \begin{matrix} H_1(s)W_1(s) \\ H_2(s)W_2(s) \end{matrix} \right\|_\infty \leq 1 \tag{1.13}$$
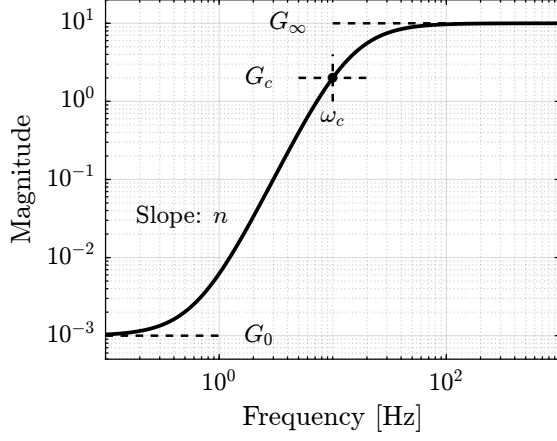
Therefore, applying the $\mathcal{H}_\infty$ synthesis to the standard plant $P(s)$ (1.10) will generate two filters $H_2(s)$ and $H_1(s) \triangleq 1 - H_2(s)$ that are complementary (1.9) and such that there norms are bellow specified bounds (1.9b), (1.9c).

Note that there is only an implication between the $\mathcal{H}_\infty$ norm condition (1.13) and the initial synthesis objectives (1.9b) and (1.9c) and not an equivalence. Hence, the optimization may be a little bit conservative with respect to the set of filters on which it is performed, see [43, Chap. 2.8.3].

Weighting Functions Design   Weighting functions are used during the synthesis to specify the maximum allowed complementary filters' norm. The proper design of these weighting functions is of primary importance for the success of the presented $\mathcal{H}_\infty$ synthesis of complementary filters.

First, only proper and stable transfer functions should be used. Second, the order of the weighting functions should stay reasonably small in order to reduce the computational costs associated with the solving of the optimization problem and for the physical implementation of the filters (the synthesized filters' order being equal to the sum of the weighting functions' order). Third, one should not forget the fundamental limitations imposed by the complementary property (1.1). This implies for instance that $|H_1(j\omega)|$ and $|H_2(j\omega)|$ cannot be made small at the same frequency.

When designing complementary filters, it is usually desired to specify their slopes, their "blending" frequency and their maximum gains at low and high frequency. To easily express these specifications, formula (1.14) is proposed to help with the design of weighting functions. The parameters in formula (1.14) are $G_0 = \lim_{\omega \to 0} |W(j\omega)|$ the low frequency gain, $G_\infty = \lim_{\omega \to \infty} |W(j\omega)|$ the high frequency gain, $G_c = |W(j\omega_c)|$ the gain at a specific frequency ω_c in rad/s and n the slope between high and low frequency, which also corresponds to the order of the weighting function. The typical magnitude of a weighting function generated using (1.14) is shown in Figure 1.8.

$$W(s) = \left(\frac{\frac{1}{\omega_c}\sqrt{\frac{1-\left(\frac{G_0}{G_c}\right)^{\frac{2}{n}}}{1-\left(\frac{G_c}{G_\infty}\right)^{\frac{2}{n}}}}s + \left(\frac{G_0}{G_c}\right)^{\frac{1}{n}}}{\left(\frac{1}{G_\infty}\right)^{\frac{1}{n}}\frac{1}{\omega_c}\sqrt{\frac{1-\left(\frac{G_0}{G_c}\right)^{\frac{2}{n}}}{1-\left(\frac{G_c}{G_\infty}\right)^{\frac{2}{n}}}}s + \left(\frac{1}{G_c}\right)^{\frac{1}{n}}} \right)^n \tag{1.14}$$

Figure 1.8: Magnitude of a weighting function generated using (1.14), $G_0 = 10^{-3}$, $G_\infty = 10$, $\omega_c = 10Hz$, $G_c = 2$, $n = 3$.

Validation of the proposed synthesis method The proposed methodology for the design of complementary filters is now applied on a simple example. Let's suppose two complementary filters $H_1(s)$ and $H_2(s)$ have to be designed such that:

- the blending frequency is around $10Hz$.

- the slope of $|H_1(j\omega)|$ is $+2$ below $10Hz$. Its low frequency gain is 10^{-3}.

- the slope of $|H_2(j\omega)|$ is -3 above $10Hz$. Its high frequency gain is 10^{-3}.

The first step is to translate the above requirements by properly designing the weighting functions. The proposed formula (1.14) is here used for such purpose. Parameters used are summarized in Table 1.2. The inverse magnitudes of the designed weighting functions, which are representing the maximum allowed norms of the complementary filters, are shown by the dashed lines in Figure 1.9.

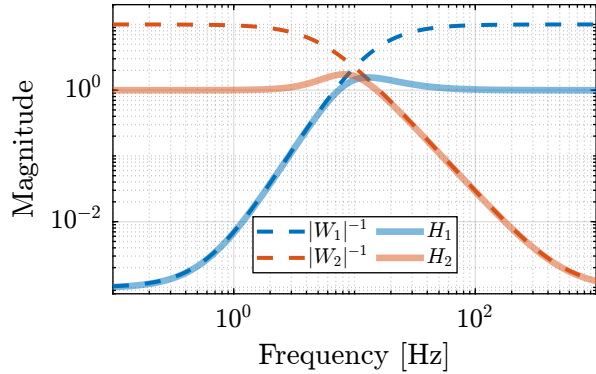| Parameter	$W_1(s)$	$W_2(s)$
G_0	0.1	1000
G_∞	1000	0.1
ω_c	$2\pi \cdot 10$	$2\pi \cdot 10$
G_c	0.45	0.45
n	2	3

Table 1.2: Parameters for $W_1(s)$ and $W_2(s)$

Figure 1.9: Weights and obtained filters

The standard $\mathcal{H}_\infty$ synthesis is then applied to the generalized plant of Figure 1.7a. The filter $H_2(s)$ that minimizes the $\mathcal{H}_\infty$ norm between w and $[z_1, \ z_2]^T$ is obtained. The $\mathcal{H}_\infty$ norm is here found to be close to one which indicates that the synthesis is successful: the complementary filters norms are below

the maximum specified upper bounds. This is confirmed by the bode plots of the obtained complementary filters in Figure 1.9. This simple example illustrates the fact that the proposed methodology for complementary filters shaping is easy to use and effective.

1.4 Synthesis of a set of three complementary filters

Some applications may require to merge more than two sensors [37], [40]. For instance at the LIGO, three sensors (an LVDT, a seismometer and a geophone) are merged to form a super sensor [41].

When merging $n > 2$ sensors using complementary filters, two architectures can be used as shown in Figure 1.10. The fusion can either be done in a "sequential" way where $n-1$ sets of two complementary filters are used (Figure 1.10a), or in a "parallel" way where one set of n complementary filters is used (Figure 1.10b).

In the first case, typical sensor fusion synthesis techniques can be used. However, when a parallel architecture is used, a new synthesis method for a set of more than two complementary filters is required as only simple analytical formulas have been proposed in the literature [37], [40]. A generalization of the proposed synthesis method of complementary filters is presented in this section.
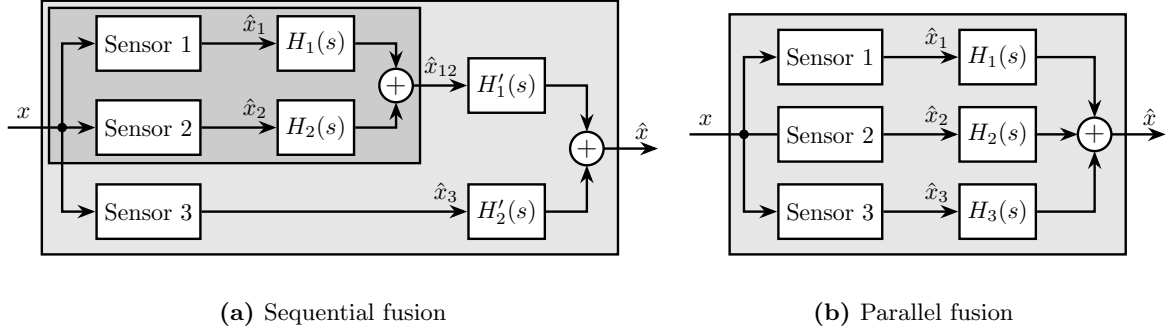

(a) Sequential fusion

(b) Parallel fusion

Figure 1.10: Possible sensor fusion architecture when more than two sensors are to be merged

The synthesis objective is to compute a set of n stable transfer functions $[H_1(s),\ H_2(s),\ \ldots,\ H_n(s)]$ such that conditions (1.15a) and (1.15b) are satisfied.

$$\sum_{i=1}^{n} H_i(s) = 1 \tag{1.15a}$$

$$|H_i(j\omega)| < \frac{1}{|W_i(j\omega)|}, \quad \forall \omega, \ i = 1 \ldots n \tag{1.15b}$$

$[W_1(s),\ W_2(s),\ \ldots,\ W_n(s)]$ are weighting transfer functions that are chosen to specify the maximum complementary filters' norm during the synthesis.

Such synthesis objective is closely related to the one described in Section 1.3, and indeed the proposed synthesis method is a generalization of the one previously presented. A set of n complementary filters can be shaped by applying the standard $\mathcal{H}_\infty$ synthesis to the generalized plant $P_n(s)$ described by (1.16).

$$
\begin{bmatrix} z_1 \\ \vdots \\ z_n \\ v \end{bmatrix} = P_n(s) \begin{bmatrix} w \\ u_1 \\ \vdots \\ u_{n-1} \end{bmatrix} ; \quad P_n(s) = \begin{bmatrix} W_1 & -W_1 & \dots & \dots & -W_1 \\ 0 & W_2 & 0 & \dots & 0 \\ \vdots & \ddots & \ddots & \ddots & \vdots \\ \vdots & & \ddots & \ddots & 0 \\ 0 & \dots & \dots & 0 & W_n \\ 1 & 0 & \dots & \dots & 0 \end{bmatrix} \tag{1.16}
$$

If the synthesis if successful, a set of $n-1$ filters $[H_2(s), H_3(s), \ldots, H_n(s)]$ are obtained such that (1.17) is verified.

$$
\left\| \begin{matrix} (1 - [H_2(s) + H_3(s) + \cdots + H_n(s)]) \, W_1(s) \\ H_2(s) W_2(s) \\ \vdots \\ H_n(s) W_n(s) \end{matrix} \right\|_\infty \leq 1 \tag{1.17}
$$

$H_1(s)$ is then defined using (1.18) which is ensuring the complementary property for the set of n filters (1.15a). Condition (1.15b) is satisfied thanks to (1.17).

$$
H_1(s) \triangleq 1 - \big[H_2(s) + H_3(s) + \cdots + H_n(s) \big] \tag{1.18}
$$

An example is given to validate the proposed method for the synthesis of a set of three complementary filters. The sensors to be merged are a displacement sensor from DC up to $1Hz$, a geophone from 1 to $10Hz$ and an accelerometer above $10Hz$. Three weighting functions are designed using formula (1.14) and their inverse magnitude are shown in Figure 1.11b (dashed curves).

Consider the generalized plant $P_3(s)$ shown in Figure 1.11a which is also described by (1.19).

$$
\begin{bmatrix} z_1 \\ z_2 \\ z_3 \\ v \end{bmatrix} = P_3(s) \begin{bmatrix} w \\ u_1 \\ u_2 \end{bmatrix} ; \quad P_3(s) = \begin{bmatrix} W_1(s) & -W_1(s) & -W_1(s) \\ 0 & W_2(s) & 0 \\ 0 & 0 & W_3(s) \\ 1 & 0 & 0 \end{bmatrix} \tag{1.19}
$$

The standard $\mathcal{H}_\infty$ synthesis is performed on the generalized plant $P_3(s)$. Two filters $H_2(s)$ and $H_3(s)$ are obtained such that the $\mathcal{H}_\infty$ norm of the closed-loop transfer from w to $[z_1, \, z_2, \, z_3]$ of the system in Figure 1.11a is less than one. Filter $H_1(s)$ is defined using (1.20) thus ensuring the complementary property of the obtained set of filters.

$$
H_1(s) \triangleq 1 - \big[H_2(s) + H_3(s) \big] \tag{1.20}
$$

Figure 1.11b displays the three synthesized complementary filters (solid lines) which confirms that the synthesis is successful.
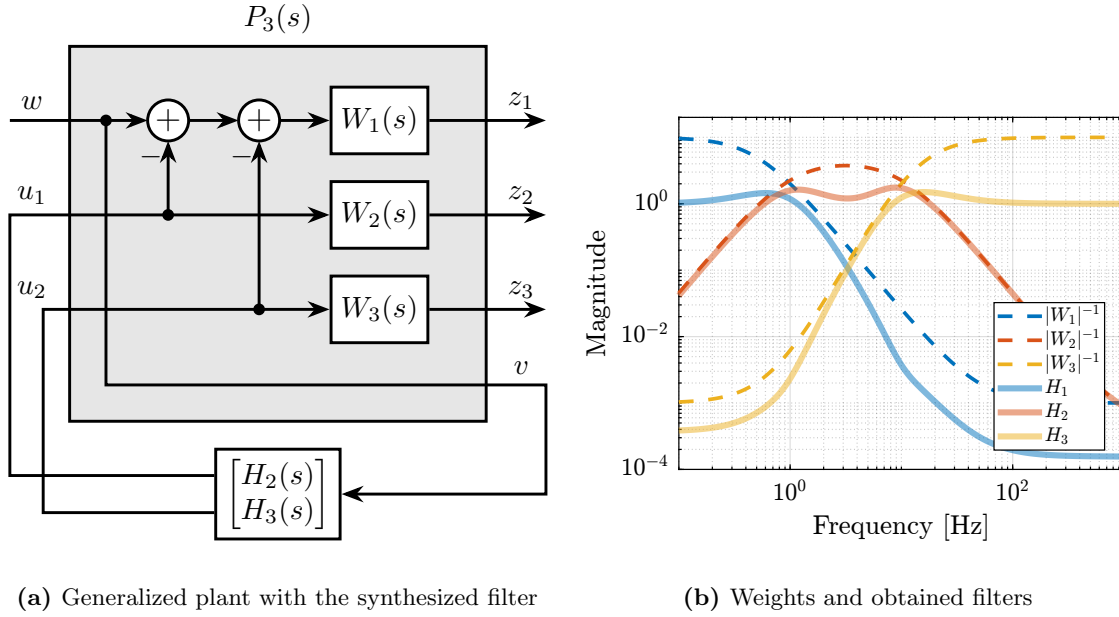
(a) Generalized plant with the synthesized filter

(b) Weights and obtained filters

Figure 1.11: Architecture for the $\mathcal{H}_\infty$ synthesis of three complementary filters (a). Bode plot of the inverse weighting functions and of the three obtained complementary filters (b)

Conclusion

A new method for designing complementary filters using the $\mathcal{H}_\infty$ synthesis has been proposed. It allows to shape the magnitude of the filters by the use of weighting functions during the synthesis. This is very valuable in practice as the characteristics of the super sensor are linked to the complementary filters' magnitude. Therefore typical sensor fusion objectives can be translated into requirements on the magnitudes of the filters. Several examples were used to emphasize the simplicity and the effectiveness of the proposed method.

However, the shaping of the complementary filters' magnitude does not allow to directly optimize the super sensor noise and dynamical characteristics. Future work will aim at developing a complementary filter synthesis method that minimizes the super sensor noise while ensuring the robustness of the fusion.

- Talk about the possibility to use H2 to minimize the RMS value of the super sensor noise? (or maybe make a section about that?) There is a draft paper about that.

- For the NASS, it was shown that the HAC-IFF strategy works fine and is easy to understand and tune

- It would be very interesting to see how sensor fusion (probably between the force sensor and the external metrology) compares in term of performance and robustness

2 Decoupling

When dealing with MIMO systems, a typical strategy is to:

- First decouple the plant dynamics (discussed in this section)

- Apply SISO control for the decoupled plant (discussed in section 3)

Another strategy would be to apply a multivariable control synthesis to the coupled system. Strangely, while H-infinity synthesis is a mature technology, it use for the control of Stewart platform is not yet demonstrated. From [14]:

> xperimental closed-loop control results using the hexapod have shown that controllers designed using a decentralized single-strut design work well when compared to full multivariable methodologies.

☒ Review of Decoupling Strategies for stewart platforms

☐ Add some citations about different methods

☐ Maybe transform table into text

Table 2.1: Litterature review about decoupling strategy for Stewart platform control

Actuators	Sensors	Control
APA	Eddy current displacement	**Decentralized** (struts) PI + LPF control
PZT	Strain Gauge	Decentralized position feedback
Piezo		
Voice Coil	Force	**Cartesian frame** decoupling
Voice Coil	Force	Cartesian Frame, Jacobians, IFF
Hydraulic	LVDT	Decentralized (strut) vs Centralized (cartesian)
Voice Coil	Accelerometer (collocated), ext. Rx/Ry sensors	Cartesian acceleration feedback (isolation) + 2DoF pointing control (external sens
Voice Coil	Accelerometer in each leg	Centralized Vibration Control, PI, Skyhook
Voice Coil	Geophone + Eddy Current (Struts, collocated)	Decentralized (Sky Hook) + Centralized (**modal**) Control
Piezoelectric	Force, Position	Vibration isolation, Model-Based, **Modal control**: 6x PI controllers
PZT	Geophone (struts)	**H-Infinity** and mu-synthesis
Voice Coil	Force sensors (struts) + accelerometer (cartesian)	Decentralized Force Feedback + Centralized H2 control based on accelerometers
Voice Coil	Accelerometers	MIMO H-Infinity, active damping

The goal of this section is to compare the use of several methods for the decoupling of parallel manipulators.
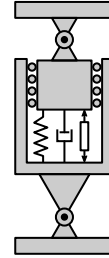
It is structured as follow:

2.1 Test Model

- Instead of comparing the decoupling strategies using the Stewart platform, a similar yet much simpler parallel manipulator is used instead

- to render the analysis simpler, the system of Figure 2.1 is used

- It has 3DoF, and has 3 parallels struts whose model is shown in Figure 2.1b

- It is quite similar to the Stewart platform (parallel architecture, as many struts as DoF)

Two frames are defined:

- $\{M\}$ with origin O_M at the Center of mass of the solid body

- $\{K\}$ with origin O_K at the Center of mass of the parallel manipulator
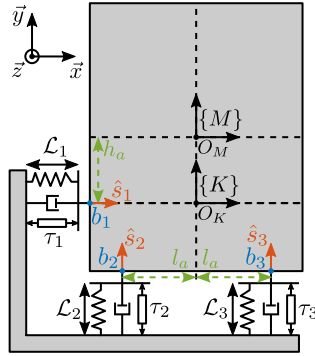
(a) Geometrical parameters   **(b)** Strut model

Figure 2.1: 3DoF model used to study decoupling strategies

First, the equation of motion are derived. Expressing the second law of Newton on the suspended mass, expressed at its center of mass gives

$$M_{\{M\}}\ddot{\boldsymbol{\mathcal{X}}}_{\{M\}}(t) = \sum \boldsymbol{\mathcal{F}}_{\{M\}}(t) \tag{2.1}$$

with $\boldsymbol{\mathcal{X}}_{\{M\}}$ the two translation and one rotation expressed with respect to the center of mass and $\boldsymbol{\mathcal{F}}_{\{M\}}$ forces and torque applied at the center of mass.

$$\boldsymbol{\mathcal{X}}_{\{M\}} = \begin{bmatrix} x \\ y \\ R_z \end{bmatrix}, \quad \boldsymbol{\mathcal{F}}_{\{M\}} = \begin{bmatrix} F_x \\ F_y \\ M_z \end{bmatrix} \tag{2.2}$$

In order to map the spring, damping and actuator forces to XY forces and Z torque expressed at the center of mass, the Jacobian matrix $\boldsymbol{J}_{\{M\}}$ is used.

$$\boldsymbol{J}_{\{M\}} = \begin{bmatrix} 1 & 0 & h_a \\ 0 & 1 & -l_a \\ 0 & 1 & l_a \end{bmatrix} \tag{2.3}$$

Then, the equation of motion linking the actuator forces τ to the motion of the mass $\boldsymbol{\mathcal{X}}_{\{M\}}$ is obtained.

$$M_{\{M\}}\ddot{\boldsymbol{\mathcal{X}}}_{\{M\}}(t) + \boldsymbol{J}_{\{M\}}^t \boldsymbol{\mathcal{C}} \boldsymbol{J}_{\{M\}} \dot{\boldsymbol{\mathcal{X}}}_{\{M\}}(t) + \boldsymbol{J}_{\{M\}}^t \boldsymbol{\mathcal{K}} \boldsymbol{J}_{\{M\}} \boldsymbol{\mathcal{X}}_{\{M\}}(t) = \boldsymbol{J}_{\{M\}}^t \boldsymbol{\tau}(t) \tag{2.4}$$

Matrices representing the payload inertia as well as the actuator stiffness and damping are shown in

$$\boldsymbol{M}_{\{M\}} = \begin{bmatrix} m & 0 & 0 \\ 0 & m & 0 \\ 0 & 0 & I \end{bmatrix}, \quad \boldsymbol{\mathcal{K}} = \begin{bmatrix} k & 0 & 0 \\ 0 & k & 0 \\ 0 & 0 & k \end{bmatrix}, \quad \boldsymbol{\mathcal{C}} = \begin{bmatrix} c & 0 & 0 \\ 0 & c & 0 \\ 0 & 0 & c \end{bmatrix} \tag{2.5}$$

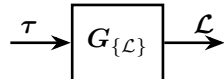Parameters used for the following analysis are summarized in table 2.2.

Table 2.2: Model parameters

Parameter	Description	Value
l_a		$0.5\,m$
h_a		$0.2\,m$
k	Actuator stiffness	$10\,N/\mu m$
c	Actuator damping	$200\,Ns/m$
m	Payload mass	$40\,\text{kg}$
I	Payload rotational inertia	$5\,\text{kg}m^2$

2.2 Control in the frame of the struts

Let's first study the obtained dynamics in the frame of the struts. The equation of motion linking actuator forces $\boldsymbol{\tau}$ to strut relative motion $\boldsymbol{\mathcal{L}}$ is obtained from (2.4) by mapping the cartesian motion of the mass to the relative motion of the struts using the Jacobian matrix $\boldsymbol{J}_{\{M\}}$ (2.3) .

The transfer function from $\boldsymbol{\tau}$ to $\boldsymbol{\mathcal{L}}$ is shown in equation (2.6).

$$\xrightarrow{\ \boldsymbol{\tau}\ } \boxed{G_{\{\mathcal{L}\}}} \xrightarrow{\ \boldsymbol{\mathcal{L}}\ }$$

$$\frac{\mathcal{L}}{\boldsymbol{\tau}}(s) = \boldsymbol{G}_{\mathcal{L}}(s) = \left(\boldsymbol{J}_{\{M\}}^{-t} M_{\{M\}} \boldsymbol{J}_{\{M\}}^{-1} s^2 + \boldsymbol{\mathcal{C}} s + \boldsymbol{\mathcal{K}} \right)^{-1} \tag{2.6}$$

At low frequency the plant converges to a diagonal constant matrix whose diagonal elements are linked to the actuator stiffnesses (2.7).

$$\boldsymbol{G}_{\mathcal{L}}(j\omega) \xrightarrow[\omega \to 0]{} \boldsymbol{\mathcal{K}}^{-1} \tag{2.7}$$

At high frequency, the plant converges to the mass matrix mapped in the frame of the struts, which is in general highly non-diagonal.

The magnitude of the coupled plant $\boldsymbol{G}_{\mathcal{L}}$ is shown in Figure 2.2. This confirms that at low frequency (below the first suspension mode), the plant is well decoupled. Depending on the symmetry in the system, some diagonal elements may be equal (such as for struts 2 and 3 in this example).
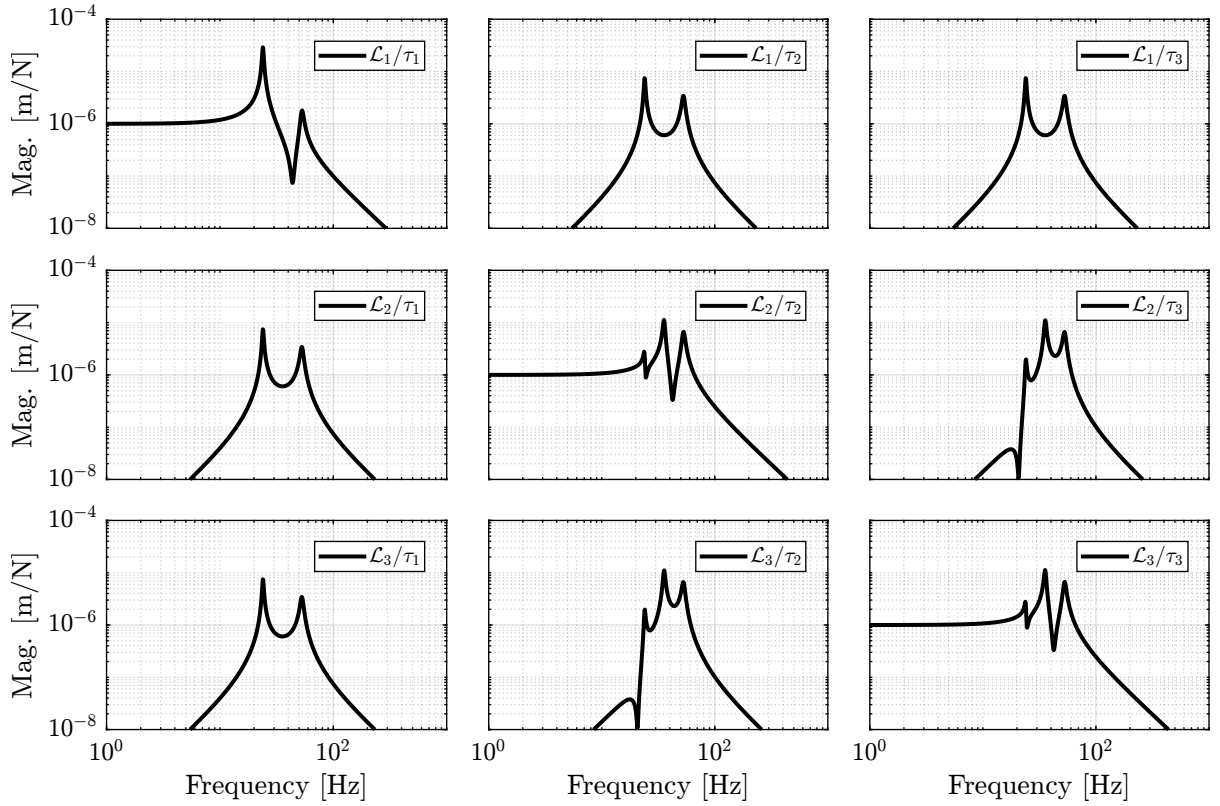

Figure 2.2: Magnitude of the coupled plant.

2.3 Jacobian Decoupling

Jacobian Matrix As already explained, the Jacobian matrix can be used to both convert strut velocity $\dot{\mathcal{L}}$ to payload velocity and angular velocity $\dot{\boldsymbol{\mathcal{X}}}_{\{O\}}$ and Convert actuators forces $\boldsymbol{\tau}$ to forces/torque applied on the payload $\boldsymbol{\mathcal{F}}_{\{O\}}$ (2.8).

$$\dot{\boldsymbol{\mathcal{X}}}_{\{O\}} = J_{\{O\}}\dot{\boldsymbol{\mathcal{L}}}, \quad \dot{\boldsymbol{\mathcal{L}}} = J_{\{O\}}^{-1}\dot{\boldsymbol{\mathcal{X}}}_{\{O\}} \tag{2.8a}$$

$$\boldsymbol{\mathcal{F}}_{\{O\}} = J_{\{O\}}^{t}\boldsymbol{\tau}, \quad \boldsymbol{\tau} = J_{\{O\}}^{-t}\boldsymbol{\mathcal{F}}_{\{O\}} \tag{2.8b}$$

The obtained plan (Figure 2.3) has inputs and outputs that have physical meaning:

- $\boldsymbol{\mathcal{F}}_{\{O\}}$ are forces/torques applied on the payload at the origin of frame $\{O\}$

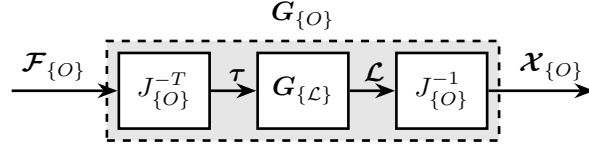- $\boldsymbol{\mathcal{X}}_{\{O\}}$ are translations/rotation of the payload expressed in frame $\{O\}$

Figure 2.3: Block diagram of the transfer function from $\boldsymbol{\mathcal{F}}_{\{O\}}$ to $\boldsymbol{\mathcal{X}}_{\{O\}}$

$$\frac{\boldsymbol{\mathcal{X}}_{\{O\}}}{\boldsymbol{\mathcal{F}}_{\{O\}}}(s) = \boldsymbol{G}_{\{O\}}(s) = \left(\boldsymbol{J}_{\{O\}}^{t}\boldsymbol{J}_{\{M\}}^{-T}\boldsymbol{M}_{\{M\}}\boldsymbol{J}_{\{M\}}^{-1}\boldsymbol{J}_{\{O\}}s^{2} + \boldsymbol{J}_{\{O\}}^{t}\boldsymbol{\mathcal{C}}\boldsymbol{J}_{\{O\}}s + \boldsymbol{J}_{\{O\}}^{t}\boldsymbol{\mathcal{K}}\boldsymbol{J}_{\{O\}} \right)^{-1} \tag{2.9}$$

The frame $\{O\}$ can be any chosen frame, but the decoupling properties depends on the chosen frame $\{O\}$. There are two natural choices: the center of mass $\{M\}$ and the center of stiffness $\{K\}$. Note that the Jacobian matrix is only based on the geometry of the system and does not depend on the physical properties such as mass and stiffness.

Center Of Mass   If the center of mass is chosen as the decoupling frame. The Jacobian matrix and its inverse are expressed in (2.10).

$$J_{\{M\}} = \begin{bmatrix} 1 & 0 & h_a \\ 0 & 1 & -l_a \\ 0 & 1 & l_a \end{bmatrix}, \quad J_{\{M\}}^{-1} = \begin{bmatrix} 1 & \frac{h_a}{2l_a} & \frac{-h_a}{2l_a} \\ 0 & \frac{1}{2} & \frac{1}{2} \\ 0 & \frac{-1}{2l_a} & \frac{1}{2l_a} \end{bmatrix} \tag{2.10}$$
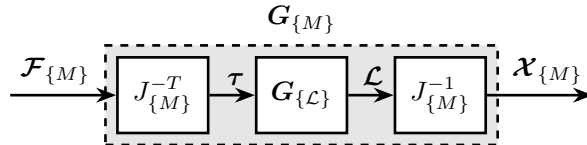
Analytical formula of the plant is (2.11).

$$\frac{\boldsymbol{\mathcal{X}}_{\{M\}}}{\boldsymbol{\mathcal{F}}_{\{M\}}}(s) = \boldsymbol{G}_{\{M\}}(s) = \left(\boldsymbol{M}_{\{M\}}s^{2} + \boldsymbol{J}_{\{M\}}^{t}\boldsymbol{\mathcal{C}}\boldsymbol{J}_{\{M\}}s + \boldsymbol{J}_{\{M\}}^{t}\boldsymbol{\mathcal{K}}\boldsymbol{J}_{\{M\}} \right)^{-1} \tag{2.11}$$

At high frequency, converges towards the inverse of the mass matrix, which is a diagonal matrix (2.12).

$$\boldsymbol{G}_{\{M\}}(j\omega) \xrightarrow[\omega\to\infty]{} -\omega^2 \boldsymbol{M}_{\{M\}}^{-1} = -\omega^2 \begin{bmatrix} 1/m & 0 & 0 \\ 0 & 1/m & 0 \\ 0 & 0 & 1/I \end{bmatrix} \quad (2.12)$$

Plant is therefore well decoupled above the suspension mode with the highest frequency. Such strategy is usually applied on systems with low frequency suspension modes, such that the plant corresponds to decoupled mass lines.

☐ Reference to some papers about vibration isolation or ASML?

The coupling at low frequency can easily be understood physically. When a static (or with frequency lower than the suspension modes) force is applied at the center of mass, rotation is induced by the stiffness of the first actuator, not in line with the force application point. this is illustrated in Figure 2.4b.
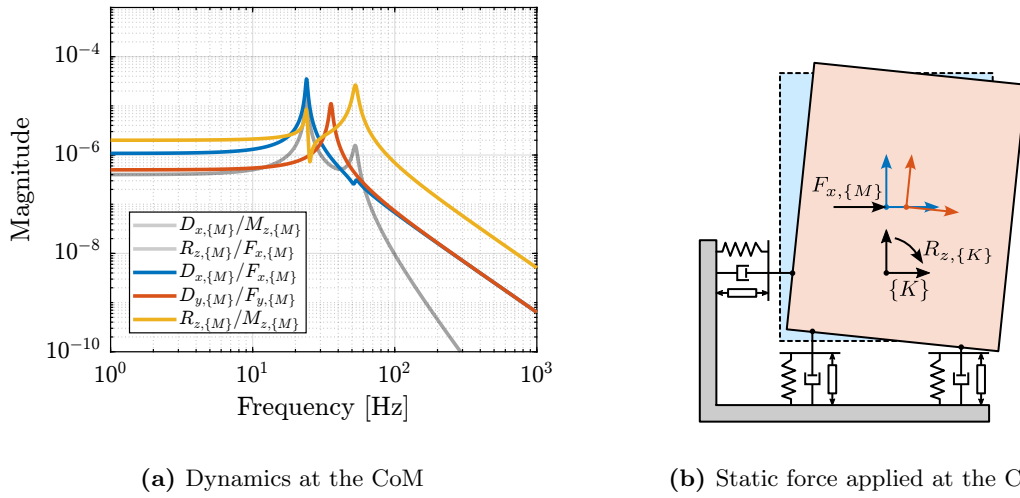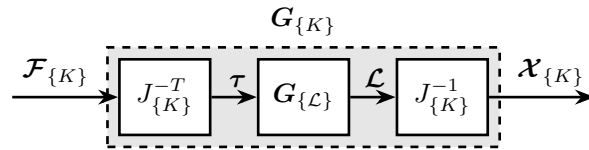

(a) Dynamics at the CoM

(b) Static force applied at the CoM

Figure 2.4: Plant decoupled using the Jacobian matrix expresssed at the center of mass (a). The physical reason for low frequency coupling is illustrated in (b).

Center Of Stiffness

$$J_{\{K\}} = \begin{bmatrix} 1 & 0 & 0 \\ 0 & 1 & -l_a \\ 0 & 1 & l_a \end{bmatrix}, \quad J_{\{K\}}^{-1} = \begin{bmatrix} 1 & 0 & 0 \\ 0 & \frac{1}{2} & \frac{1}{2} \\ 0 & \frac{-1}{2l_a} & \frac{1}{2l_a} \end{bmatrix} \quad (2.13)$$

Frame $\{K\}$ is chosen such that $\boldsymbol{J}_{\{K\}}^t \boldsymbol{\mathcal{K}} \boldsymbol{J}_{\{K\}}$ is diagonal. Typically, it can me made based on physical reasoning as is the case here.

$$\frac{\boldsymbol{\mathcal{X}}_{\{K\}}}{\boldsymbol{\mathcal{F}}_{\{K\}}}(s) = \boldsymbol{G}_{\{K\}}(s) = \left(\boldsymbol{J}_{\{K\}}^t \boldsymbol{J}_{\{M\}}^{-T} \boldsymbol{M}_{\{M\}} \boldsymbol{J}_{\{M\}}^{-1} \boldsymbol{J}_{\{K\}} s^2 + \boldsymbol{J}_{\{K\}}^t \boldsymbol{\mathcal{C}} \boldsymbol{J}_{\{K\}} s + \boldsymbol{J}_{\{K\}}^t \boldsymbol{\mathcal{K}} \boldsymbol{J}_{\{K\}} \right)^{-1} \quad (2.14)$$
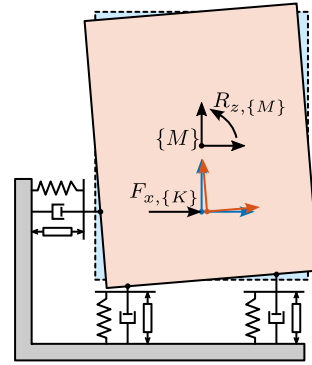
Plant is well decoupled below the suspension mode with the lowest frequency. This is usually suited for systems which high stiffness.

$$\boldsymbol{G}_{\{K\}}(j\omega) \xrightarrow[\omega \to 0]{} \boldsymbol{J}_{\{K\}}^{-1} \boldsymbol{\mathcal{K}}^{-1} \boldsymbol{J}_{\{K\}}^{-t} \quad (2.15)$$

☐ Make a schematic where the thing is deformed at high frequency rotating about the center of mass
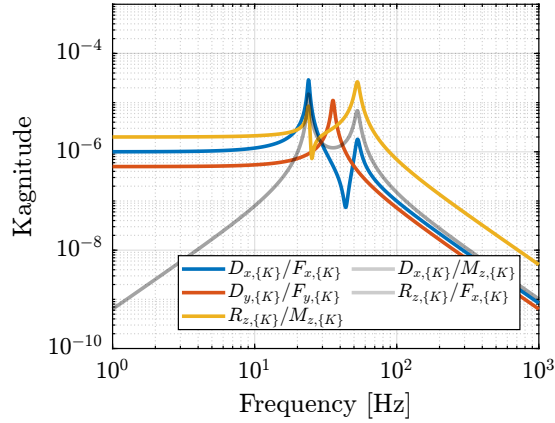
(a) Dynamics at the CoK

(b) High frequency force applied at the CoK

Figure 2.5: Plant decoupled using the Jacobian matrix expresssed at the center of stiffness (a). The physical reason for low frequency coupling is illustrated in (b).

2.4 Modal Decoupling

Let's consider a system with the following equations of motion:

$$M\ddot{\boldsymbol{x}} + C\dot{\boldsymbol{x}} + K\boldsymbol{x} = \boldsymbol{\mathcal{F}} \quad (2.16)$$

And the measurement output is a combination of the motion variable $\boldsymbol{x}$:

$$\boldsymbol{y} = C_{ox}\boldsymbol{x} + C_{ov}\dot{\boldsymbol{x}} \quad (2.17)$$

Let's make a **change of variables**:

$$\boxed{\boldsymbol{x} = \Phi \boldsymbol{x}_m} \quad (2.18)$$

with:

- $\boldsymbol{x}_m$ the modal amplitudes

23

- Φ a matrix whose columns are the modes shapes of the system

And we map the actuator forces:

$$\boldsymbol{\mathcal{F}} = J^T \boldsymbol{\tau} \tag{2.19}$$

The equations of motion become:

$$M\Phi\ddot{\boldsymbol{x}}_m + C\Phi\dot{\boldsymbol{x}}_m + K\Phi\boldsymbol{x}_m = J^T\boldsymbol{\tau} \tag{2.20}$$

And the measured output is:

$$\boldsymbol{y} = C_{ox}\Phi\boldsymbol{x}_m + C_{ov}\Phi\dot{\boldsymbol{x}}_m \tag{2.21}$$

By pre-multiplying the EoM by Φ^T:

$$\Phi^T M\Phi\ddot{\boldsymbol{x}}_m + \Phi^T C\Phi\dot{\boldsymbol{x}}_m + \Phi^T K\Phi\boldsymbol{x}_m = \Phi^T J^T\boldsymbol{\tau} \tag{2.22}$$

And we note:

- $M_m = \Phi^T M\Phi = \mathrm{diag}(\mu_i)$ the modal mass matrix

- $C_m = \Phi^T C\Phi = \mathrm{diag}(2\xi_i\mu_i\omega_i)$ (classical damping)

- $K_m = \Phi^T K\Phi = \mathrm{diag}(\mu_i\omega_i^2)$ the modal stiffness matrix

And we have:

$$\ddot{\boldsymbol{x}}_m + 2\Xi\Omega\dot{\boldsymbol{x}}_m + \Omega^2\boldsymbol{x}_m = \mu^{-1}\Phi^T J^T\boldsymbol{\tau} \tag{2.23}$$

with:

- $\mu = \mathrm{diag}(\mu_i)$

- $\Omega = \mathrm{diag}(\omega_i)$

- $\Xi = \mathrm{diag}(\xi_i)$

And we call the **modal input matrix**:

$$\boxed{B_m = \mu^{-1}\Phi^T J^T} \tag{2.24}$$

And the **modal output matrices**:

$$\boxed{C_m = C_{ox}\Phi + C_{ov}\Phi s} \tag{2.25}$$

Let's note the "modal input":

$$\boldsymbol{\tau}_m = B_m\boldsymbol{\tau} \tag{2.26}$$

The transfer function from $\boldsymbol{\tau}_m$ to $\boldsymbol{x}_m$ is:

$$\boxed{\frac{\boldsymbol{x}_m}{\boldsymbol{\tau}_m} = \left(I_n s^2 + 2\Xi\Omega s + \Omega^2\right)^{-1}} \tag{2.27}$$

which is a **diagonal** transfer function matrix. We therefore have decoupling of the dynamics from $\boldsymbol{\tau}_m$ to $\boldsymbol{x}_m$.

We now expressed the transfer function from input $\boldsymbol{\tau}$ to output $\boldsymbol{y}$ as a function of the "modal variables":

$$\frac{\boldsymbol{y}}{\boldsymbol{\tau}} = \underbrace{(C_{ox} + sC_{ov})\,\Phi}_{C_m} \underbrace{\left(I_n s^2 + 2\Xi\Omega s + \Omega^2\right)^{-1}}_{\text{diagonal}} \underbrace{\left(\mu^{-1}\Phi^T J^T\right)}_{B_m} \tag{2.28}$$

By inverting B_m and C_m and using them as shown in Figure 2.6, we can see that we control the system in the "modal space" in which it is decoupled.
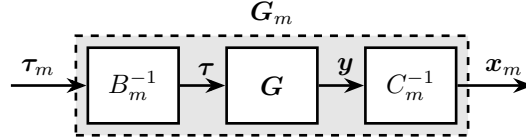

Figure 2.6: Modal Decoupling Architecture

The system $\boldsymbol{G}_m(s)$ shown in Figure 2.6 is diagonal (**??**).

Modal decoupling requires to have the equations of motion of the system. From the equations of motion (and more precisely the mass and stiffness matrices), the mode shapes Φ are computed.

Then, the system can be decoupled in the modal space. The obtained system on the diagonal are second order resonant systems which can be easily controlled.

Using this decoupling strategy, it is possible to control each mode individually.

Example   For the system in Figure 2.1a, we have:

$$\boldsymbol{x} = \begin{bmatrix} x \\ y \\ R_z \end{bmatrix} \tag{2.29}$$

$$\boldsymbol{y} = \mathcal{L} = J\boldsymbol{x}; \quad C_{ox} = J; \quad C_{ov} = 0 \tag{2.30}$$

$$M = \begin{bmatrix} m & 0 & 0 \\ 0 & m & 0 \\ 0 & 0 & I \end{bmatrix}; \quad K = J' \begin{bmatrix} k & 0 & 0 \\ 0 & k & 0 \\ 0 & 0 & k \end{bmatrix} J; \quad C = J' \begin{bmatrix} c & 0 & 0 \\ 0 & c & 0 \\ 0 & 0 & c \end{bmatrix} J \tag{2.31}$$

In order to apply the architecture shown in Figure 2.6, we need to compute C_{ox}, C_{ov}, Φ, μ and J.

☐ Is it possible to obtained the analytical formulas for decoupling matrices?

2.5 SVD Decoupling

Singular Value Decomposition

- Introduction to SVD **brunton22˙data**

- Applied to parallel manipulator?

Singular value is used a lot for multivariable control [43]. Used to study directions in multivariable systems

Control Architecture

☐ SVD controllers described in [43, chapt. 3.5.4]

☐ **Check if inverse U and V should be used or just U and V matrices**, Use correct notations.

☐ Have notation for the measured FRF and for the real approximation

$$\boldsymbol{G}(j\omega) = \begin{bmatrix} 0 & 0 & 0 \\ 0 & 0 & 0 \\ 0 & 0 & 0 \end{bmatrix} \xrightarrow[approximation]{real} \begin{bmatrix} 0 & 0 & 0 \\ 0 & 0 & 0 \\ 0 & 0 & 0 \end{bmatrix} \xrightarrow[SVD]{} U =, \ V = \tag{2.32}$$

Procedure:

- Identify the dynamics of the system from inputs to outputs (can be obtained experimentally) Frequency Response Function, which is a complex matrix obtained for several frequency points.

- Choose a frequency where we want to decouple the system (usually, the crossover frequency is a good choice)

- Compute a real approximation of the system's response at that frequency As *real* V and U matrices need to be obtained, a real approximation of the complex measured response needs to be computed. **kouvaritakis79˙theor˙pract˙charac˙locus˙desig˙method**: real matrix that preserves the most orthogonality in directions with the input complex matrix

- Perform a Singular Value Decomposition of the real approximation. Unitary U and V matrices are then obtained such that: V-t Greal U-1 is a diagonal matrix

- Use the singular input and output matrices to decouple the system as shown in Figure 2.7

$$G_{svd}(s) = U^{-1}G(s)V^{-T}$$
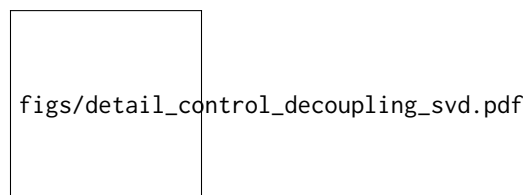

figs/detail_control_decoupling_svd.pdf

Figure 2.7: Decoupled plant $\boldsymbol{G}_{SVD}$ using the Singular Value Decomposition

In order to apply the Singular Value Decomposition, we need to have the Frequency Response Function of the system, at least near the frequency where we wish to decouple the system. The FRF can be experimentally obtained or based from a model.

This method ensure good decoupling near the chosen frequency, but no guaranteed decoupling away from this frequency.

Also, it depends on how good the real approximation of the FRF is, therefore it might be less good for plants with high damping.

This method is quite general and can be applied to any type of system. The inputs and outputs are ordered from higher gain to lower gain at the chosen frequency.

☐ Do we loose any physical meaning of the obtained inputs and outputs?

☐ Can we take advantage of the fact that U and V are unitary?

Example

☐ Analytical formulas in this case?

☐ Maybe show the complex and real response matrices.

☐ At least, show the obtained matrices

☐ Do we have something special when applying SVD to a collocated MIMO system?

- **Verify why such a good decoupling is obtained!**
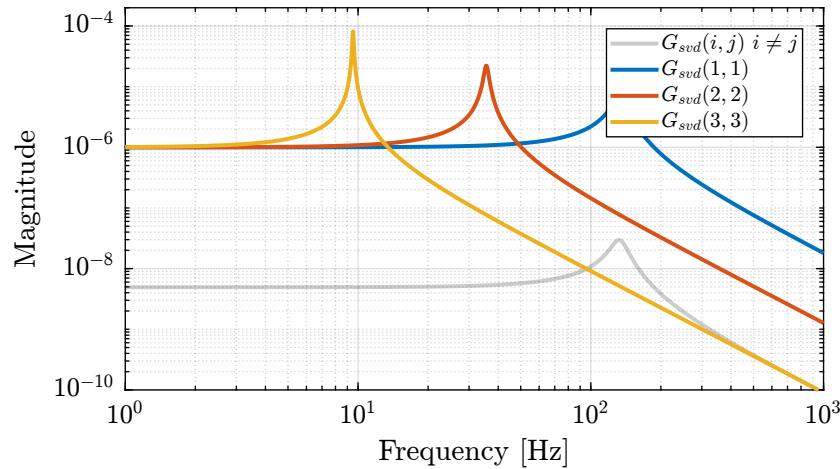
$$\boldsymbol{G}_{SVD}(s) = \tag{2.33}$$

Figure 2.8: Svd plant $G_m(s)$

Table 2.3: Real approximate of G at the decoupling frequency ω_c

-8e-06	2.1e-06	-2.1e-06
2.1e-06	-1.3e-06	-2.5e-08
-2.1e-06	-2.5e-08	-1.3e-06

27

2.6 Comparison

Table 2.4: Comparison of decoupling strategies

	Jacobian	Modal	SVD
Philosophy	Topology Driven	Physics Driven	Data Driven
Requirements	Known geometry	Known equations of motion	Identified FRF
Decoupling Matrices	Decoupling using J obtained from geometry	Decoupling using Φ obtained from modal decomposition	Decoupling using U and V obtained from SVD
Decoupled Plant	$\boldsymbol{G}_{\{O\}} = J_{\{O\}}^{-1} \boldsymbol{G} J_{\{O\}}^{-T}$	$\boldsymbol{G}_m = C_m^{-1} \boldsymbol{G} B_m^{-1}$	$\boldsymbol{G}_{svd}(s) = U^{-1} \boldsymbol{G}(s) V^{-T}$
Implemented Controller	$\boldsymbol{K}_{\{O\}} = J_{\{O\}}^{-T} \boldsymbol{K}_d(s) J_{\{O\}}^{-1}$	$\boldsymbol{K}_m = B_m^{-1} \boldsymbol{K}_d(s) C_m^{-1}$	$\boldsymbol{K}_{svd}(s) = V^{-T} \boldsymbol{K}_d(s) U^{-1}$
Physical Interpretation	Forces/Torques to Displacement/Rotation in chosen frame	Inputs to excite individual modes Output to sense individual modes	Directions of max to min controllability/observability
Decoupling Properties	Decoupling at low or high frequency depending on the chosen frame	Good decoupling at all frequencies	Good decoupling near the chosen frequency
Pros	Physical inputs / outputs Good decoupling at High frequency (diagonal mass matrix if Jacobian taken at the CoM) Good decoupling at Low frequency (if Jacobian taken at specific point) Easy integration of meaningful reference inputs	Target specific modes 2nd order diagonal plant	Good Decoupling near the crossover Very General
Cons	Coupling between force/rotation may be high at low frequency (non diagonal terms in K) Limited to parallel mechanisms (?) If good decoupling at all frequencies =¿ requires specific mechanical architecture	Need analytical equations	Loose the physical meaning of inputs /outputs Decoupling depends on the real approximation validity Diagonal plants may not be easy to control
Applicability	Parallel Mechanisms Only small motion for the Jacobian matrix to stay constant	Systems whose dynamics that can be expressed with M and K matrices	Very general Need FRF data (either experimentally or analytically)

Conclusion

The three proposed methods clearly have a lot in common as they all tend to make system more decoupled by pre and/or post multiplying by a constant matrix However, the three methods also differs by a number of points which are summarized in Table 2.4.

Other decoupling strategies could be included in this study, such as:

- DC decoupling: pre-multiply the plant by $G(0)^{-1}$

- full decoupling: pre-multiply the plant by $G(s)^{-1}$

Conclusion about NASS:

- Prefer to use Jacobian decoupling as we get more physical interpretation

- Also, it is possible to take into account different specifications in the different DoF

3 Closed-Loop Shaping using Complementary Filters

Performance of a feedback control is dictated by closed-loop transfer functions. For instance sensitivity, transmissibility, etc... Gang of Four.

There are several ways to design a controller to obtain a given performance.

Decoupled Open-Loop Shaping:

- As shown in previous section, once the plant is decoupled: open loop shaping

- Explain procedure when applying open-loop shaping

- Lead, Lag, Notches, Check Stability, c2d, etc...

- But this is open-loop shaping, and it does not directly work on the closed loop transfer functions

Other strategy: Model Based Design:

- Multivariable Control

- Talk about Caio's thesis?

- Review of model based design (LQG, H-Infinity) applied to Stewart platform

- Difficulty to specify robustness to change of payload mass

In this section, an alternative is proposed in which complementary filters are used for closed-loop shaping. It is presented for a SISO system, but can be generalized to MIMO if decoupling is sufficient. It will be experimentally demonstrated with the NASS.

Paper's introduction:

Model based control

SISO control design methods

- frequency domain techniques

- manual loop-shaping - key idea: modification of the controller such that the open-loop is made according to specifications [51]. This works well because the open loop transfer function is linearly dependent of the controller. Different techniques for open loop shaping **lurie02˙system˙archit˙trades˙using˙bode**

However, the specifications are given in terms of the final system performance, i.e. as closed-loop specifications.

Norm-based control loop-shaping [43]. Far from standard in industry as it requires lot of efforts.

Problem of robustness to plant uncertainty:

- Trade off performance / robustness. Difficult to obtain high performance in presence of high uncertainty.

- Robust control μ-synthesis. Takes a lot of effort to model the plant uncertainty.

- Sensor fusion: combines two sensors using complementary filters. The high frequency sensor is collocated with the actuator in order to ensure the stability of the system even in presence of uncertainty. [26], [52]

Complementary filters: [22].

In this paper, we propose a new controller synthesis method

- based on the use of complementary high pass and low pass filters

- inverse based control

- direct translation of requirements such as disturbance rejection and robustness to plant uncertainty

3.1 Control Architecture

Virtual Sensor Fusion Let's consider the control architecture represented in Figure 3.1 where G' is the physical plant to control, G is a model of the plant, k is a gain, H_L and H_H are complementary filters ($H_L + H_H = 1$ in the complex sense). The signals are the reference signal r, the output perturbation d_y, the measurement noise n and the control input u.
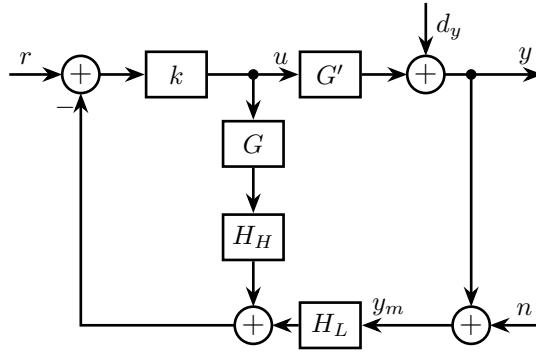

Figure 3.1: Sensor Fusion Architecture

The dynamics of the closed-loop system is described by the following equations

$$y = \frac{1 + kGH_H}{1 + L}dy + \frac{kG'}{1 + L}r - \frac{kG'H_L}{1 + L}n \tag{3.1}$$

$$u = -\frac{kH_L}{1 + L}dy \quad + \frac{k}{1 + L}r - \frac{kH_L}{1 + L}n \tag{3.2}$$

with $L = k(GH_H + G'H_L)$.

The idea of using such architecture comes from sensor fusion [26], [52] where we use two sensors. One is measuring the quantity that is required to control, the other is collocated with the actuator in such a way that stability is guaranteed. The first one is low pass filtered in order to obtain good performance at low frequencies and the second one is high pass filtered to benefits from its good dynamical properties.

Here, the second sensor is replaced by a model G of the plant which is assumed to be stable and minimum phase.

One may think that the control architecture shown in Figure 3.1 is a multi-loop system, but because no non-linear saturation-type element is present in the inner-loop (containing k, G and H_H which are all numerically implemented), the structure is equivalent to the architecture shown in Figure 3.2.
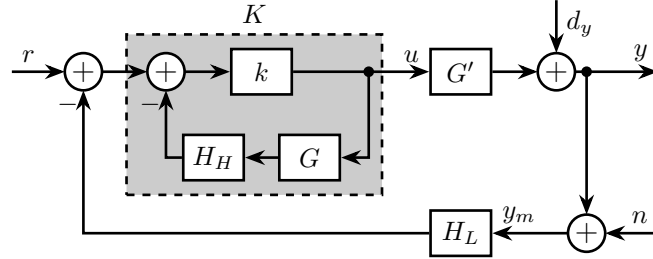

Figure 3.2: Equivalent feedback architecture

The dynamics of the system can be rewritten as follow

$$y = \frac{1}{1 + G'KH_L}dy + \frac{G'K}{1 + G'KH_L}r - \frac{G'KH_L}{1 + G'KH_L}n \tag{3.3}$$

$$u = \frac{-KH_L}{1 + G'KH_L}dy + \frac{K}{1 + G'KH_L}r - \frac{KH_L}{1 + G'KH_L}n \tag{3.4}$$

with $K = \frac{k}{1 + H_H Gk}$

Asymptotic behavior   We now want to study the asymptotic system obtained when using very high value of k

$$\lim_{k \to \infty} K = \lim_{k \to \infty} \frac{k}{1 + H_H Gk} = (H_H G)^{-1} \tag{3.5}$$

If the obtained K is improper, a low pass filter can be added to have its causal realization.

Also, we want K to be stable, so G and H_H must be minimum phase transfer functions.

For now on, we will consider the resulting control architecture as shown on Figure 3.3 where the only "tuning parameters" are the complementary filters.
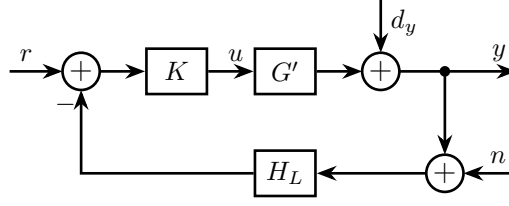
Figure 3.3: Equivalent classical feedback control architecture

The equations describing the dynamics of the closed-loop system are

$$y = \frac{H_H dy + G'G^{-1}r - G'G^{-1}H_L n}{H_H + G'G^{-1}H_L} \tag{3.6}$$

$$u = \frac{-G^{-1}H_L dy + G^{-1}r - G^{-1}H_L n}{H_H + G'G^{-1}H_L} \tag{3.7}$$

At frequencies where the model is accurate: $G^{-1}G' \approx 1$, $H_H + G'G^{-1}H_L \approx H_H + H_L = 1$ and

$$y = H_H dy + r - H_L n \tag{3.8}$$

$$u = -G^{-1}H_L dy + G^{-1}r - G^{-1}H_L n \tag{3.9}$$

We obtain a sensitivity transfer function equals to the high pass filter $S = \frac{y}{dy} = H_H$ and a transmissibility transfer function equals to the low pass filter $T = \frac{y}{n} = H_L$.

Assuming that we have a good model of the plant, we have then that the closed-loop behavior of the system converges to the designed complementary filters.

3.2 Translating the performance requirements into the shapes of the complementary filters

The required performance specifications in a feedback system can usually be translated into requirements on the upper bounds of $S(j)$ and $|T(j\omega)|$ [53]. The process of designing a controller $K(s)$ in order to obtain the desired shapes of $S(j)$ and $T(j)$ is called loop shaping.

The equations (3.6) and (3.7) describing the dynamics of the studied feedback architecture are not written in terms of K but in terms of the complementary filters H_L and H_H.

In this section, we then translate the typical specifications into the desired shapes of the complementary filters H_L and H_H.

Nominal Stability (NS) The closed-loop system is stable if all its elements are stable (K, G' and H_L) and if the sensitivity function ($S = \frac{1}{1+G'KH_L}$) is stable.

For the nominal system ($G' = G$), we have $S = H_H$.

Nominal stability is then guaranteed if H_L, H_H and G are stable and if G and H_H are minimum phase (to have K stable).

Thus we must design stable and minimum phase complementary filters.

Nominal Performance (NP)   Typical performance specifications can usually be translated into upper bounds on $|S(j\omega)|$ and $|T(j\omega)|$.

Two performance weights w_H and w_L are defined in such a way that performance specifications are satisfied if

$$|w_H(j\omega)S(j\omega)| \leq 1, \ |w_L(j\omega)T(j\omega)| \leq 1 \quad \forall \omega \tag{3.10}$$

For the nominal system, we have $S = H_H$ and $T = H_L$, and then nominal performance is ensured by requiring

NP $\Leftrightarrow |w_H(j\omega)H_H(j\omega)| \leq 1 \quad \forall \omega$
$|w_L(j\omega)H_L(j\omega)| \leq 1 \quad \forall \omega$

The translation of typical performance requirements on the shapes of the complementary filters is discussed below:

- for disturbance rejections, make $|S| = |H_H|$ small

- for noise attenuation, make $|T| = |H_L|$ small

- for control energy reduction, make $|KS| = |G^{-1}|$ small

We may have other requirements in terms of stability margins, maximum or minimum closed-loop bandwidth.

Closed-Loop Bandwidth   The closed-loop bandwidth $_B$ can be defined as the frequency where $S(j)$ first crosses $\frac{1}{\sqrt{2}}$ from below.

If one wants the closed-loop bandwidth to be at least $^*_B$ (e.g. to stabilize an unstable pole), one can required that $|S(j\omega)| \leq \frac{1}{\sqrt{2}}$ below ω_B^* by designing w_H such that $|w_H(j\omega)| \geq \sqrt{2}$ for $\omega \leq \omega_B^*$.

Similarly, if one wants the closed-loop bandwidth to be less than $^*_B$, one can approximately require that the magnitude of T is less than $\frac{1}{\sqrt{2}}$ at frequencies above $^*_B$ by designing w_L such that $|w_L(j\omega)| \geq \sqrt{2}$ for $\omega \geq \omega_B^*$.

Classical stability margins   Gain margin (GM) and phase margin (PM) are usual specifications on controlled system. Minimum GM and PM can be guaranteed by limiting the maximum magnitude of the sensibility function $M_S = \max_\omega |S(j\omega)|$:

$$\text{GM} \geq \frac{M_S}{M_S - 1}; \quad \text{PM} \geq \frac{1}{M_S} \tag{3.11}$$

Thus, having $M_S \leq 2$ guarantees a gain margin of at least 2 and a phase margin of at least 29.

For the nominal system $M_S = \max_\omega |S| = \max_\omega |H_H|$, so one can design w_H so that $|w_H(j\omega)| \geq 1/2$ in order to have

$$|H_H(j\omega)| \leq 2 \quad \forall \omega \tag{3.12}$$

and thus obtain acceptable stability margins.

Response time to change of reference signal For the nominal system, the model is accurate and the transfer function from reference signal r to output y is 1 (3.8) and does not depends of the complementary filters.

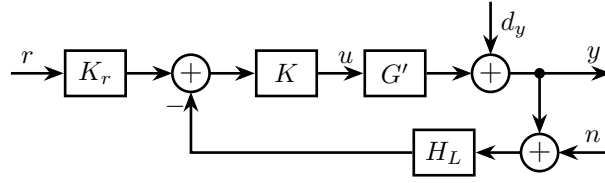However, one can add a pre-filter as shown in Figure 3.4.

Figure 3.4: Prefilter used to limit input usage

The transfer function from y to r becomes $\frac{y}{r} = K_r$ and K_r can we chosen to obtain acceptable response to change of the reference signal. Typically, K_r is a low pass filter of the form

$$K_r(s) = \frac{1}{1 + \tau s} \tag{3.13}$$

with τ corresponding to the desired response time.

Input usage Input usage due to disturbances d_y and measurement noise n is determined by $\left|\frac{u}{d_y}\right| = \left|\frac{u}{n}\right| = \left|G^{-1} H_L\right|$. Thus it can be limited by setting an upper bound on $|H_L|$.

Input usage due to reference signal r is determined by $\left|\frac{u}{r}\right| = \left|G^{-1} K_r\right|$ when using a pre-filter (Figure 3.4) and $\left|\frac{u}{r}\right| = \left|G^{-1}\right|$ otherwise.

Proper choice of $|K_r|$ is then useful to limit input usage due to change of reference signal.

Robust Stability (RS) Robustness stability represents the ability of the control system to remain stable even though there are differences between the actual system G' and the model G that was used to design the controller. These differences can have various origins such as unmodelled dynamics or non-linearities.

To represent the differences between the model and the actual system, one can choose to use the general input multiplicative uncertainty as represented in Figure 3.5.

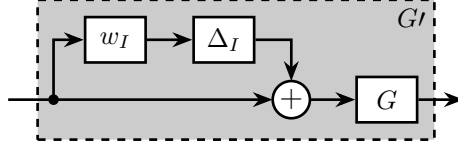Then, the set of possible perturbed plant is described by

Figure 3.5: Input multiplicative uncertainty

$$\Pi_i: \quad G_p(s) = G(s)\big(1 + w_I(s)\Delta_I(s)\big); \quad \Delta_I(j) \le 1 \ \forall \tag{3.14}$$

and w_I should be chosen such that all possible plants G' are contained in the set Π_i.

Using input multiplicative uncertainty, robust stability is equivalent to have [43]:

$$
\begin{aligned}
\text{RS} &\Leftrightarrow |w_I T| \le 1 \quad \forall G' \in \Pi_I, \ \forall \omega \\
&\Leftrightarrow \left| w_I \frac{G' K H_L}{1 + G' K H_L} \right| \le 1 \quad \forall G' \in \Pi_I, \ \forall \omega \\
&\Leftrightarrow \left| w_I \frac{G' G^{-1} H_H{}^{-1} H_L}{1 + G' G^{-1} H_H{}^{-1} H_L} \right| \le 1 \quad \forall G' \in \Pi_I, \ \forall \omega \\
&\Leftrightarrow \left| w_I \frac{(1 + w_I \Delta) H_H{}^{-1} H_L}{1 + (1 + w_I \Delta) H_H{}^{-1} H_L} \right| \le 1 \quad \forall \Delta, \ |\Delta| \le 1, \ \forall \omega \\
&\Leftrightarrow \left| w_I \frac{(1 + w_I \Delta) H_L}{1 + w_I \Delta H_L} \right| \le 1 \quad \forall \Delta, \ |\Delta| \le 1, \ \forall \omega \\
&\Leftrightarrow |H_L w_I| \frac{1 + |w_I|}{1 - |w_I H_L|} \le 1, \quad 1 - |w_I H_L| > 0 \quad \forall \omega \\
&\Leftrightarrow |H_L w_I| (2 + |w_I|) \le 1, \quad 1 - |w_I H_L| > 0 \quad \forall \omega \\
&\Leftrightarrow |H_L w_I| (2 + |w_I|) \le 1 \quad \forall \omega
\end{aligned}
$$

Robust stability is then guaranteed by having the low pass filter H_L satisfying (3.15).

$$\text{RS} \Leftrightarrow |H_L| \le \frac{1}{|w_I|(2 + |w_I|)} \quad \forall \omega \tag{3.15}$$

To ensure robust stability condition (3.2) can be used if w_L is designed in such a way that $|w_L| \ge |w_I|(2 + |w_I|)$.

Robust Performance (RP) Robust performance is a property for a controlled system to have its performance guaranteed even though the dynamics of the plant is changing within specified bounds.

For robust performance, we then require to have the performance condition valid for all possible plants in the defined uncertainty set: RP $\Leftrightarrow |w_H S| \le 1 \quad \forall G' \in \Pi_I, \ \forall \omega$
$|w_L T| \le 1 \quad \forall G' \in \Pi_I, \ \forall \omega$

Let's transform condition (3.2) into a condition on the complementary filters

$$|w_H S| \leq 1 \quad \forall G' \in \Pi_I, \ \forall \omega$$

$$\Leftrightarrow \left| w_H \frac{1}{1 + G'G^{-1}H_H^{-1}H_L} \right| \leq 1 \quad \forall G' \in \Pi_I, \ \forall \omega$$

$$\Leftrightarrow \left| \frac{w_H H_H}{1 + \Delta w_I H_L} \right| \leq 1 \quad \forall \Delta, \ |\Delta| \leq 1, \ \forall \omega$$

$$\Leftrightarrow \frac{|w_H H_H|}{1 - |w_I H_L|} \leq 1, \ \forall \omega$$

$$\Leftrightarrow |w_H H_H| + |w_I H_L| \leq 1, \ \forall \omega$$

The same can be done with condition (3.2)

$$|w_L T| \leq 1 \quad \forall G' \in \Pi_I, \ \forall \omega$$

$$\Leftrightarrow \left| w_L \frac{G'G^{-1}H_H^{-1}H_L}{1 + G'G^{-1}H_H^{-1}H_L} \right| \leq 1 \quad \forall G' \in \Pi_I, \ \forall \omega$$

$$\Leftrightarrow \left| w_L H_L \frac{1 + w_I \Delta}{1 + w_I \Delta H_L} \right| \leq 1 \quad \forall \Delta, \ |\Delta| \leq 1, \ \forall \omega$$

$$\Leftrightarrow |w_L H_L| \frac{1 + |w_I|}{1 - |w_I H_L|} \leq 1 \quad \forall \omega$$

$$\Leftrightarrow |H_L| \leq \frac{1}{|w_L|(1 + |w_I|) + |w_I|} \quad \forall \omega$$

Robust performance is then guaranteed if (3.2) and (3.2) are satisfied.

RP $\Leftrightarrow |w_H H_H| + |w_I H_L| \leq 1, \ \forall \omega$
$|H_L| \leq \frac{1}{|w_L|(1+|w_I|)+|w_I|} \quad \forall \omega$

One should be aware than when looking for a robust performance condition, only the worst case is evaluated and using the robust stability condition may lead to conservative control.

3.3 Analytical formulas for complementary filters?

3.4 Numerical Example

Procedure   In order to apply this control technique, we propose the following procedure:

1. Identify the plant to be controlled in order to obtain G

2. Design the weighting function w_I such that all possible plants G' are contained in the set Π_i

3. Translate the performance requirements into upper bounds on the complementary filters (as explained in Sec. 3.2)

4. Design the weighting functions w_H and w_L and generate the complementary filters using -synthesis (as further explained in Sec. 1.3). If the synthesis fails to give filters satisfying the upper bounds previously defined, either the requirements have to be reworked or a better model G that will permits to have a smaller w_I should be obtained. If one does not want to use the $\mathcal{H}_\infty$ synthesis, one can use pre-made complementary filters given in Sec. 3.3.

5. If $K = (GH_H)^{-1}$ is not proper, a low pass filter should be added

6. Design a pre-filter K_r if requirements on input usage or response to reference change are not met

7. Control implementation: Filter the measurement with H_L, implement the controller K and the pre-filter K_r as shown on Figure 3.4

Plant Let's consider the problem of controlling an active vibration isolation system that consist of a mass m to be isolated, a piezoelectric actuator and a geophone.

We represent this system by a mass-spring-damper system as shown Figure 3.6 where m typically represents the mass of the payload to be isolated, k and c represent respectively the stiffness and damping of the mount. w is the ground motion. The values for the parameters of the models are

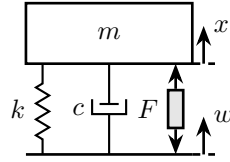$$m = 20; \quad k = 10^4/; \quad c = 10^2()$$

Figure 3.6: Model of the positioning system

The model of the plant $G(s)$ from actuator force F to displacement x is then

$$G(s) = \frac{1}{ms^2 + cs + k} \tag{3.16}$$

Its bode plot is shown on Figure 3.7.

Requirements The control objective is to isolate the displacement x of the mass from the ground motion w.

The disturbance rejection should be at least 10 at 2 and with a slope of -2 below 2 until a rejection of 10^4.

Closed-loop bandwidth should be less than 20 (because of time delay induced by limited sampling frequency?).

Noise attenuation should be at least 10 above 40 and 100 above 500

Robustness to unmodelled dynamics. We model the uncertainty on the dynamics of the plant by a multiplicative weight

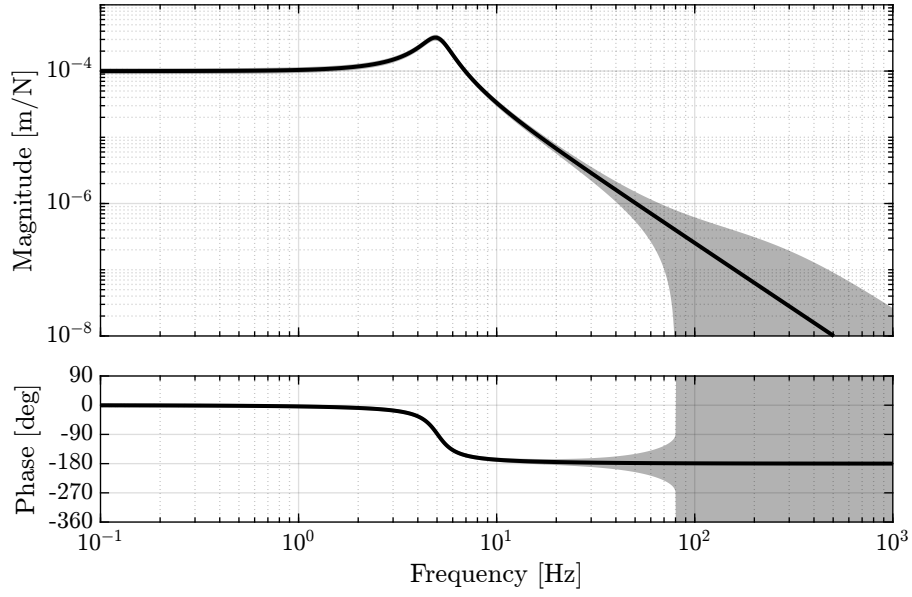$$w_I(s) = \frac{\tau s + r_0}{(\tau/r_\infty)s + 1} \tag{3.17}$$

**Figure 3.7:** Bode plot of the transfer function $G(s)$ from F to x

where $r_0 = 0.1$ is the relative uncertainty at steady-state, $1/\tau = 100$ is the frequency at which the relative uncertainty reaches 100, and $r_\infty = 10$ is the magnitude of the weight at high frequency.

All the requirements on H_L and H_H are represented on Figure 3.8a.

☐ TODO: Make Matlab code to plot the specifications
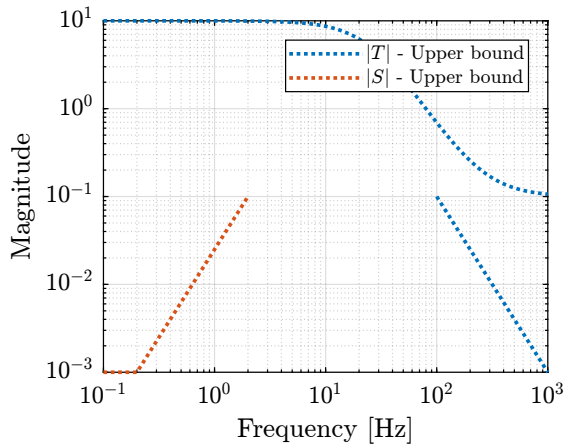
(a) Closed loop specifications
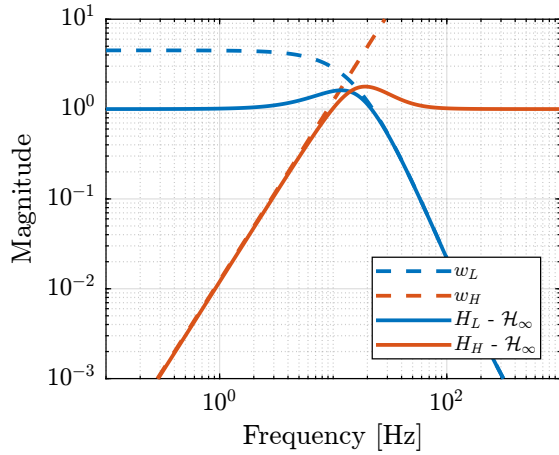
(b) Obtained complementary filters

Figure 3.8: Caption with reference to sub figure (a) (b)

Design of the filters Or maybe use analytical formulas as proposed here: Complementary filters using analytical formula

We then design w_L and w_H such that their magnitude are below the upper bounds shown on Figure 3.8b.

$$w_L = \frac{(s + 22.36)^2}{0.005(s + 1000)^2} \tag{3.18a}$$

$$w_H = \frac{1}{0.0005(s + 0.4472)^2} \tag{3.18b}$$

After the -synthesis, we obtain H_L and H_H, and we plot their magnitude on phase on Figure 3.8b.

$$H_L = \frac{0.0063957(s + 1016)(s + 985.4)(s + 26.99)}{(s + 57.99)(s^2 + 65.77s + 2981)} \tag{3.19a}$$

$$H_H = \frac{0.9936(s + 111.1)(s^2 + 0.3988s + 0.08464)}{(s + 57.99)(s^2 + 65.77s + 2981)} \tag{3.19b}$$

Controller analysis The controller is $K = (H_H G)^{-1}$. A low pass filter is added to K so that it is proper and implementable.

The obtained controller is shown on Figure 3.10a.
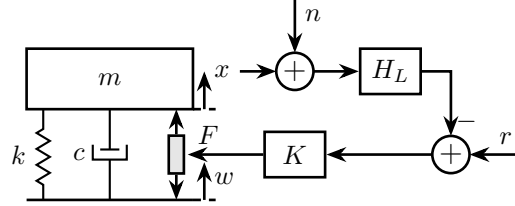
It is implemented as shown on Figure 3.9.

Figure 3.9: Control of a positioning system

Robustness analysis The robust stability can be access on the nyquist plot (Figure 3.11a).

The robust performance is shown on Figure 3.11b.

## 3.5 Experimental Validation?

Experimental Validation

Conclusion

☐ Discuss how useful it is as the bandwidth can be changed in real time with analytical formulas of second order complementary filters. Maybe make a section about that. Maybe give analytical formulas of second order complementary filters in the digital domain?
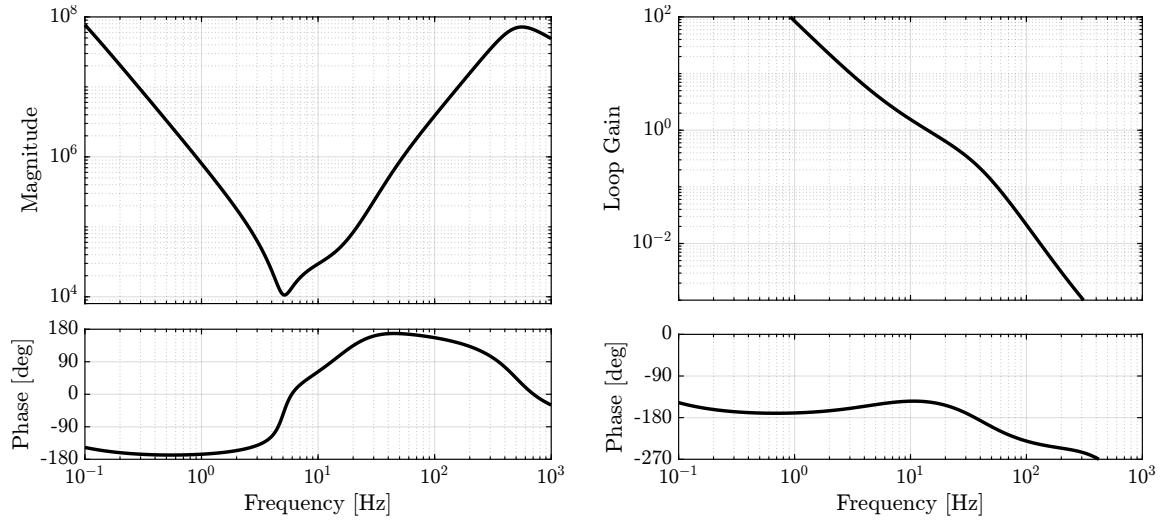
(a) Controller K

(b) Loop Gain

Figure 3.10: Caption with reference to sub figure (a) (b)
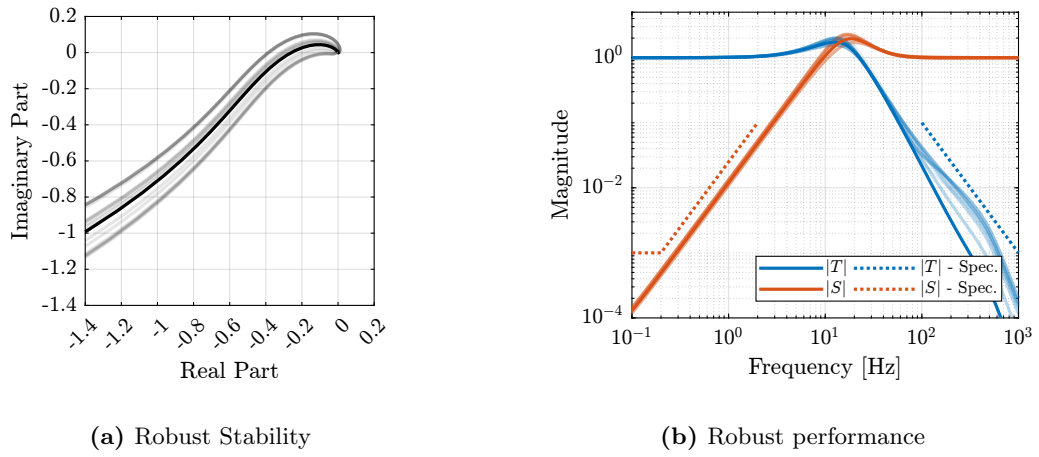
(a) Robust Stability

(b) Robust performance

Figure 3.11: Caption with reference to sub figure (a) (b)

☐ Say that it will be validated with the nano-hexapod

☐ Disadvantages:

- not optimal

- computationally intensive?

- lead to inverse control which may not be wanted in many cases. Add reference.

Conclusion

Bibliography

[1]   Z. J. Geng, G. G. Pan, L. S. Haynes, B. K. Wada, and J. A. Garba, "An intelligent control system for multiple degree-of-freedom vibration isolation," *Journal of Intelligent Material Systems and Structures*, vol. 6, no. 6, pp. 787–800, 1995 (cit. on pp. 4, 5).

[2]   A. Preumont, *Vibration Control of Active Structures - Fourth Edition* (Solid Mechanics and Its Applications). Springer International Publishing, 2018 (cit. on p. 4).

[3]   C. Wang, X. Xie, Y. Chen, and Z. Zhang, "Investigation on active vibration isolation of a stewart platform with piezoelectric actuators," *Journal of Sound and Vibration*, vol. 383, pp. 1–19, Nov. 2016 (cit. on pp. 4, 5).

[4]   X. Li, J. C. Hamann, and J. E. McInroy, "Simultaneous vibration isolation and pointing control of flexure jointed hexapods," in *Smart Structures and Materials 2001: Smart Structures and Integrated Systems*, Aug. 2001 (cit. on pp. 4, 5, 17).

[5]   H. Pu, X. Chen, Z. Zhou, and X. Luo, "Six-degree-of-freedom active vibration isolation system with decoupled collocated control," *Proceedings of the Institution of Mechanical Engineers, Part B: Journal of Engineering Manufacture*, vol. 226, no. 2, pp. 313–325, 2011 (cit. on pp. 4, 5, 17).

[6]   X. Xie, C. Wang, and Z. Zhang, "Modeling and control of a hybrid passive/active stewart vibration isolation platform," in *INTER-NOISE and NOISE-CON Congress and Conference Proceedings*, Institute of Noise Control Engineering, vol. 255, 2017, pp. 1844–1853 (cit. on pp. 4, 5, 17).

[7]   D. Tjepkema, "Active hard mount vibration isolation for precision equipment [ph. d. thesis]," Ph.D. dissertation, 2012 (cit. on pp. 4, 5).

[8]   D. Tjepkema, J. van Dijk, and H. Soemers, "Sensor fusion for active vibration isolation in precision equipment," *Journal of Sound and Vibration*, vol. 331, no. 4, pp. 735–749, 2012 (cit. on pp. 4–6).

[9]   G. Hauge and M. Campbell, "Sensors and control of a space-based six-axis vibration isolation system," *Journal of Sound and Vibration*, vol. 269, no. 3-5, pp. 913–931, 2004 (cit. on pp. 4, 5).

[10]   M. A. Beijen, D. Tjepkema, and J. van Dijk, "Two-sensor control in active vibration isolation using hard mounts," *Control Engineering Practice*, vol. 26, pp. 82–90, 2014 (cit. on p. 4).

[11]   Y. K. Yong and A. J. Fleming, "High-speed vertical positioning stage with integrated dual-sensor arrangement," *Sensors and Actuators A: Physical*, vol. 248, pp. 184–192, 2016 (cit. on pp. 4, 6, 7).

[12]   X. Yang, H. Wu, B. Chen, S. Kang, and S. Cheng, "Dynamic modeling and decoupled control of a flexible stewart platform for vibration isolation," *Journal of Sound and Vibration*, vol. 439, pp. 398–412, Jan. 2019 (cit. on pp. 5, 17).

[13]   D. Thayer and J. Vagners, "A look at the pole/zero structure of a stewart platform using special coordinate basis," in *Proceedings of the 1998 American Control Conference. ACC (IEEE Cat. No.98CH36207)*, 1998 (cit. on p. 5).

[14]   D. Thayer, M. Campbell, J. Vagners, and A. von Flotow, "Six-axis vibration isolation system using soft actuators and multiple sensors," *Journal of Spacecraft and Rockets*, vol. 39, no. 2, pp. 206–212, 2002 (cit. on pp. 5, 17).

[15] J. McInroy, "Dynamic modeling of flexure jointed hexapods for control purposes," in *Proceedings of the 1999 IEEE International Conference on Control Applications (Cat. No.99CH36328)*, 1999 (cit. on pp. 5, 17).

[16] J. McInroy, J. O'Brien, and G. Neat, "Precise, fault-tolerant pointing using a stewart platform," *IEEE/ASME Transactions on Mechatronics*, vol. 4, no. 1, pp. 91–95, 1999 (cit. on pp. 5, 17).

[17] J. McInroy and J. Hamann, "Design and control of flexure jointed hexapods," *IEEE Transactions on Robotics and Automation*, vol. 16, no. 4, pp. 372–381, 2000 (cit. on pp. 5, 17).

[18] J. Bendat, "Optimum filters for independent measurements of two related perturbed messages," *IRE Transactions on Circuit Theory*, 1957 (cit. on p. 6).

[19] F. Shaw and K. Srinivasan, "Bandwidth enhancement of position measurements using measured acceleration," *Mechanical Systems and Signal Processing*, vol. 4, no. 1, pp. 23–38, 1990 (cit. on pp. 6, 7).

[20] M. Zimmermann and W. Sulzer, "High bandwidth orientation measurement and control based on complementary filtering," *Robot Control 1991*, Robot Control 1991, pp. 525–530, 1992 (cit. on pp. 6, 7).

[21] H. G. Min and E. T. Jeung, "Complementary filter design for angle estimation using mems accelerometer and gyroscope," *Department of Control and Instrumentation, Changwon National University, Changwon, Korea*, pp. 641–773, 2015 (cit. on pp. 6, 7).

[22] W. Hua, "Low frequency vibration isolation and alignment system for advanced ligo," Ph.D. dissertation, stanford university, 2005 (cit. on pp. 6, 7, 31).

[23] W. Hua, D. B. Debra, C. T. Hardham, B. T. Lantz, and J. A. Giaime, "Polyphase fir complementary filters for control systems," in *Proceedings of ASPE Spring Topical Meeting on Control of Precision Systems*, 2004, pp. 109–114 (cit. on pp. 6, 7).

[24] A. R. Plummer, "Optimal complementary filters and their application in motion measurement," *Proceedings of the Institution of Mechanical Engineers, Part I: Journal of Systems and Control Engineering*, vol. 220, no. 6, pp. 489–507, 2006 (cit. on pp. 6, 7).

[25] P. Y. C. H. Robert Grover Brown, *Introduction to Random Signals and Applied Kalman Filtering with Matlab Exercises*, 4th ed. Wiley, 2012 (cit. on p. 6).

[26] C. Collette and F. Matichard, "Sensor fusion methods for high performance active vibration isolation systems," *Journal of Sound and Vibration*, vol. 342, pp. 1–21, 2015 (cit. on pp. 6, 7, 31, 32).

[27] A.-J. Baerveldt and R. Klang, "A low-cost and low-weight attitude estimation system for an autonomous helicopter," in *Proceedings of IEEE International Conference on Intelligent Engineering Systems*, 1997 (cit. on pp. 6, 7).

[28] P. Corke, "An inertial and visual sensing system for a small autonomous helicopter," *Journal of Robotic Systems*, vol. 21, no. 2, pp. 43–51, 2004 (cit. on pp. 6, 7).

[29] A. Jensen, C. Coopmans, and Y. Chen, "Basics and guidelines of complementary filters for small uas navigation," in *2013 International Conference on Unmanned Aircraft Systems (ICUAS)*, May 2013 (cit. on pp. 6, 7).

[30] A. Pascoal, I. Kaminer, and P. Oliveira, "Navigation system design using time-varying complementary filters," in *Guidance, Navigation, and Control Conference and Exhibit*, 1999 (cit. on pp. 6, 7).

[31] P. Batista, C. Silvestre, and P. Oliveira, "Optimal position and velocity navigation filters for autonomous vehicles," *Automatica*, vol. 46, no. 4, pp. 767–774, 2010 (cit. on p. 6).

[32] J. van Heijningen, "Low-frequency performance improvement of seismic attenuation systems and vibration sensors for next generation gravitational wave detectors," Ph.D. dissertation, Vrije Universiteit, 2018 (cit. on p. 6).

[33] T. Lucia, "Low frequency optimization and performance of advanced virgo seismic isolation system," Ph.D. dissertation, University of Siena, 2018 (cit. on p. 6).

[34] W. Anderson and E. Fritze, "Instrument approach system steering computer," *Proceedings of the IRE*, vol. 41, no. 2, pp. 219–228, 1953 (cit. on p. 6).

[35] R. G. Brown, "Integrated navigation systems and kalman filtering: A perspective," *Navigation*, vol. 19, no. 4, pp. 355–362, 1972 (cit. on p. 6).

[36] W. T. Higgins, "A comparison of complementary and kalman filtering," *IEEE Transactions on Aerospace and Electronic Systems*, no. 3, pp. 321–325, 1975 (cit. on p. 6).

[37] F. P. N. da Fonseca Cardoso, J. M. F. Calado, C. B. Cardeira, P. J. C. R. Oliveira, et al., "Complementary filter design with three frequency bands: Robot attitude estimation," in *2015 IEEE International Conference on Autonomous Robot Systems and Competitions*, IEEE, 2015, pp. 168–173 (cit. on pp. 6, 7, 14).

[38] S. I. Moore, A. J. Fleming, and Y. K. Yong, "Capacitive instrumentation and sensor fusion for high-bandwidth nanopositioning," *IEEE Sensors Letters*, vol. 3, no. 8, pp. 1–3, 2019 (cit. on p. 6).

[39] T.-J. Yeh, C.-Y. Su, and W.-J. Wang, "Modelling and control of a hydraulically actuated two-degree-of-freedom inertial platform," *Proceedings of the Institution of Mechanical Engineers, Part I: Journal of Systems and Control Engineering*, vol. 219, no. 6, pp. 405–417, 2005 (cit. on p. 7).

[40] D. Stoten, "Fusion of kinetic data using composite filters," *Proceedings of the Institution of Mechanical Engineers, Part I: Journal of Systems and Control Engineering*, vol. 215, no. 5, pp. 483–497, 2001 (cit. on pp. 7, 14).

[41] F. Matichard, B. Lantz, R. Mittleman, et al., "Seismic isolation of advanced ligo: Review of strategy, instrumentation and performance," *Classical and Quantum Gravity*, vol. 32, no. 18, p. 185 003, 2015 (cit. on pp. 7, 14).

[42] T. Dehaeze, M. Vermat, and C. Collette, "Complementary filters shaping using $\mathcal{H}_\infty$ synthesis," in *7th International Conference on Control, Mechatronics and Automation (ICCMA)*, 2019, pp. 459–464 (cit. on p. 7).

[43] S. Skogestad and I. Postlethwaite, *Multivariable Feedback Control: Analysis and Design - Second Edition*. John Wiley, 2007 (cit. on pp. 12, 26, 31, 36).

[44] K. Furutani, M. Suzuki, and R. Kudoh, "Nanometre-cutting machine using a stewart-platform parallel mechanism," *Measurement Science and Technology*, vol. 15, no. 2, pp. 467–474, 2004 (cit. on p. 17).

[45] Z. Du, R. Shi, and W. Dong, "A piezo-actuated high-precision flexible parallel pointing mechanism: Conceptual design, development, and experiments," *IEEE Transactions on Robotics*, vol. 30, no. 1, pp. 131–137, 2014 (cit. on p. 17).

[46] J. O'Brien, J. McInroy, D. Bodtke, M. Bruch, and J. Hamann, "Lessons learned in nonlinear systems and flexible robots through experiments on a 6 legged platform," in *Proceedings of the 1998 American Control Conference. ACC (IEEE Cat. No.98CH36207)*, 1998 (cit. on p. 17).

[47] D. H. Kim, J.-Y. Kang, and K.-I. Lee, "Robust tracking control design for a 6 dof parallel manipulator," *Journal of Robotic Systems*, vol. 17, no. 10, pp. 527–547, 2000 (cit. on p. 17).

[48] H. Abbas and H. Hai, "Vibration isolation concepts for non-cubic stewart platform using modal control," in *Proceedings of 2014 11th International Bhurban Conference on Applied Sciences & Technology (IBCAST) Islamabad, Pakistan, 14th - 18th January, 2014*, Jan. 2014 (cit. on p. 17).

[49] L. Lei and W. Benli, "Multi objective robust active vibration control for flexure jointed struts of stewart platforms via H_∞ and μ synthesis," *Chinese Journal of Aeronautics*, vol. 21, no. 2, pp. 125–133, 2008 (cit. on p. 17).

[50] J. Jiao, Y. Wu, K. Yu, and R. Zhao, "Dynamic modeling and experimental analyses of stewart platform with flexible hinges," *Journal of Vibration and Control*, vol. 25, no. 1, pp. 151–171, 2018 (cit. on p. 17).

[51] T. Oomen, "Advanced motion control for precision mechatronics: Control, identification, and learning of complex systems," *IEEJ Journal of Industry Applications*, vol. 7, no. 2, pp. 127–140, 2018 (cit. on p. 30).

[52] C. Collette and F. Matichard, "Vibration control of flexible structures using fusion of inertial sensors and hyper-stable actuator-sensor pairs," in *International Conference on Noise and Vibration Engineering (ISMA2014)*, 2014 (cit. on pp. 31, 32).

[53] J. E. Bibel and D. S. Malyevac, "Guidelines for the selection of weighting functions for h-infinity control," NAVAL SURFACE WARFARE CENTER DAHLGREN DIV VA, Tech. Rep., 1992 (cit. on p. 33).